Review

Metal sulfide-based Z-scheme heterojunctions in photocatalytic removal ofcontaminants, H_2 evolution and CO_2 reduction: Current status and future perspectives

Fang Deng [a,*], Junlong Peng [a], Xibao Li [a], Xubiao Luo [a,***], Priyanka Ganguly [b], Suresh C. Pillai [c], Bangxing Ren [d], Lin Ding [a], Dionysios D. Dionysiou [d,**]

[a] National-Local Joint Engineering Research Center of Heavy Metal Pollutants Control and Resource Utilization, Nanchang Hangkong University, Nanchang, 330063, PR China

[b] Chemical and Pharmaceutical Sciences, School of Human Sciences, London Metropolitan University, N78DB, London, UK

[c] Nanotechnology and Bio-Engineering Research Group, Department of Environmental Sciences, Atlantic Technological University, ATU Sligo, F91 YW50, Ireland

[d] Environmental Engineering and Science Program, Department of Chemical and Environmental Engineering (DBCEE), University of Cincinnati, Cincinnati, OH, 45221- 0012, USA

A B S T R A C T

Metal sulfides are promising photocatalysts in virtue of inherent photoelectric properties and wide light ab- sorption range. However, metal sulfides are usually subjected to photocorrosion and high carrier recombination. The assembly of metal sulfide-based Z-scheme heterojunctions not only can overcome the above shortcomings of metal sulfides, but also maintain optimum redox performance. This review will provide an overview on the general properties of metal sulfides, three different types and synthesis methods of metal sulfide-based Z-scheme heterojunctions. Most importantly, the photocatalytic mechanism originating from the internal electric field was discussed from the Fermi level, direction of charge transfer and generation of reactive species. The applications of metal sulfide-based Z-scheme heterojunctions in decomposing organic contaminants, hydrogen (H_2) evolution and carbon dioxide (CO_2) reduction were also summed up. In the end, the challenges and outlooks of sulfide- based Z-scheme heterojunctions were presented.

1. Introduction

The rapid industrialization, socioeconomic growth and the improvement of human living standards have potentially contributed to environmental pollution and energy shortages, which have garnered significant global concern (Sun et al., 2020; Xiao et al., 2019; Huang et al., 2018; Jiang, 2016; Jin et al., 2020). To handle the environmental problem and depletion of fossil fuels, it is pressing to exploit renewable energy resources and develop feasible technologies for environmental remediation (Loeb et al., 2019; Wang et al., 2018a; Zhu et al., 2020; Singh et al., 2020; Ong et al., 2016). Solar energy is perceived as one ofthe most prospective alternative energy in virtue of its clean, renewable and abundant characteristics (Li et al., 2016a, 2021a; Xu et al., 2022a; Xia et al., 2019). However, the capture and storage of solar energy are big challenges. Thus, it is essential to transform solar energy to another form that is sustainable, clean, eco-friendly, and easy to store and transport.

Until now, tremendous efforts have been put forth to transform solar energy to applicable energy via various strategies, such as solar cells (Kim et al., 2020; Zhen et al., 2019), photoelectrochemical cells (Scheuermann and Mclntyre, 2016; Zeng et al., 2018a) and photo- catalysis (Meng et al., 2016; Zhou et al., 2021). Among them, photo- catalysis has been dismissed as a prospective technology for photoconversion in virtue of its potential in solar utilization for hydrogen (H_2) production and some carbonaceous fuels such as methanol (CH_3OH), methane (CH_4), formic acid (HCOOH) and formaldehyde (HCHO) (Alberto et al., 2018; Hao et al., 2018; Li et al., 2021b; Tianet al., 2020). Moreover, photocatalytic technology is an effective and sustainable alternative for environmental pollution control due to its several merits such as ease of operation, high treatment efficiency, low energy consumption and simple equipment (Fang et al., 2020; Zhu and Wang, 2017; Osterloh, 2018; Cai et al., 2019). Nevertheless, the photocatalytic performance is limited by the following contradictory conditions: (1) the energy of available photons ($h\nu$) should be higher thanthe energy gap (E_g) (Zhu and Zhou, 2021; Deng et al., 2020), which indicates that narrow E_g is conducive to the utilization of sunlight; (2)the redox potential of reaction should be situated between the valence band (VB) top and conduction band (CB) bottom (Luo et al., 2017a),which means that more positive VB and more negative CB are thermo- dynamically beneficial to redox reaction (Hu et al., 2018). Therefore, the single-component photocatalysts hardly have strong redox capability and good light absorption in wide range. Moreover, they are usually subjected to easy recombination of photogenerated electrons (e^-) with holes (h^+) in VB (Fig. 1a), which can be attenuated by designing suitable type II heterojunctions (Wang et al., 2013). In type II heterojunctions,the migration of excited e^- in the CB of catalyst (S2) to CB of catalyst(S1) and the transfer of h^+ in the VB of S1 to the VB of S2 (Fig. 1b) accelerate separation of photogenerated e^- and h^+ (Paul et al., 2019; Dashtian et al., 2018). This charge transfer process results in attenuated oxidation and reduction abilities (Low et al., 2017), and electrostatic repulsion between the same kind of charges is ignored. It is hard for type II heterojunctions to achieve broad range of light absorption, effective carrier separation and strong redox capability simultaneously. There-fore, it is essential to exploit appropriate catalytic systems to solve the problems listed above.

In nature, the distinctive structure of green plants enables them to make effective use of solar energy, and transform CO_2 and water into carbohydrates and oxygen (O_2). The production of O_2 and reducing coenzyme occurs in two different parts of chloroplasts, and these two processes occur simultaneously (Qi et al., 2018). The charge migrationin this process occurs as similar to the English letter 'Z'. Recently, re- searchers have carried out some exploratory work on fabrication of such photocatalytic systems by simulating the photosynthesis of green plants in nature. Successful Z-scheme photocatalysts include CdS/Co_9S_8 (Qiu et al., 2017a), P-MoS_2@WO_3 (Wei et al., 2021), LaTiO2N/Bi2S3 (Sharma et al., 2020), etc. In Z-scheme photocatalytic systems, the separation efficiency of photogenerated carriers is significantly improved, light-absorption response range is widened, and strong redox ability is maintained. Thus, fabricating Z-scheme photocatalytic systems appears a pertinent strategy to realize optimal charge separation and increase photocatalytic activity. Amongst different categories of nano- materials and their composites used as photocatalysts, metal sulfides are considered as promising adsorbents and photocatalysts for removal of pollutants, H_2 production and CO_2 reduction. In the last decade, therehave been several excellent reviews on sulfide-based compounds (Shenet al., 2023; Yu et al., 2016; Chandrasekaran et al., 2019). These reviews emphasized energy storage, energy conversion and photocatalytic ap-plications. This review sums up the latest advance of metal sulfide-based Z-scheme photocatalytic systems, which includes the properties of metal sulfide, common types and synthetic methods of Z-scheme photo- catalysts, underlying photocatalytic mechanism and applications in the decomposition of pollutants, hydrogen production and CO_2 reduction (Fig. 2).

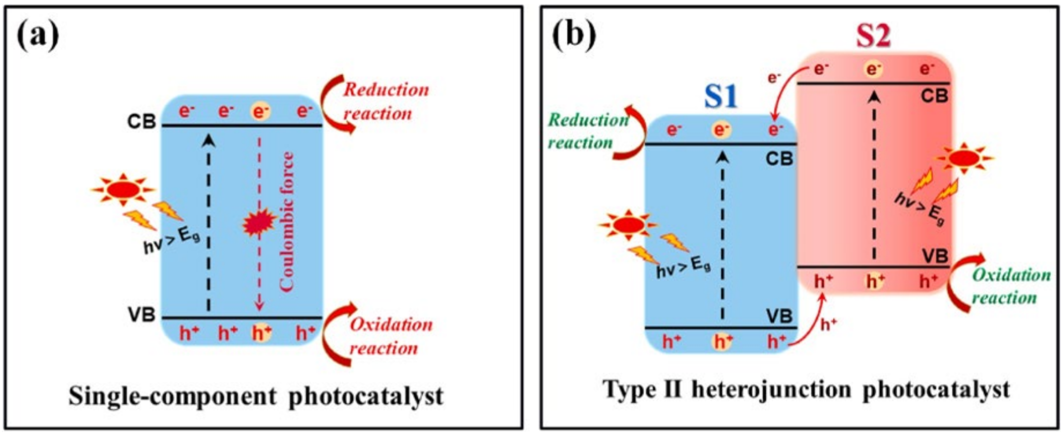

Fig. 1. Charge transfer in (a) single-component photocatalyst and (b) type II heterojunction photocatalytic system.

2. The properties of metal sulfide

Binary metallic sulfide compounds have sulfur anion combining with metallic cation to form MS, M_2S, M_3S_4 and several other stoichiometries. Binary metal sulfides, including cadmium sulfide (CdS) and zinc sulfide (ZnS), are regarded as promising photocatalysts due to their appropriate band gap value (E_g), wide light absorption range, inherent electrical properties and efficient photocatalytic activity (Lee and Wu, 2017; Cheng et al., 2018). CdS, with a medium E_g of 2.4 eV, is widely used in photocatalytic decomposition of organic contaminants, H_2 generation and CO_2 reduction under visible light (Ai et al., 2018; Feng et al., 2021). ZnS has a wide E_g of 3.6 eV, and only responds to ultraviolet light and cannot realize high visible-light photocatalytic activity (Ahluwalia et al., 2016). Layered SnS_2 with a narrow E_g of 1.91−2.35 eV (Li et al., 2016b) shows visible-light response and low toxicity, which makes SnS_2 as visible-light photocatalysts. However, binary metal sulfides usually have poor stability and are prone to photo-corrosion under light. For example, when CdS is used for photocatalytic decomposition of organic pollut-ants, the photo-corrosion is severe and the catalytic performance decreases rapidly as the reaction continues (Wang et al., 2019a). Moreover, the swift recombination of photogenerated e^- and h^+ restricts its wide application (Sun et al., 2018a). Therefore, the design and syn- thesis of metal sulfides with visible-light absorption, good stability and high photocatalytic performance have become research hotspots.

Multi-component metal chalcogenides have the characteristics of good stability, narrow band gap, high photoconductivity, strong visible- light response and low toxicity (Friedrich et al., 2017). The early application of multi-component metal chalcogenides was focused on solar cells, photoelectric and photochemical devices, nonlinear opticalmaterials and light-emitting diodes. The excellent properties of multi-component chalcogenides make them promising visible-light-responsive photocatalysts (Hu et al., 2015). Some I-III-VI and II-III-VI ternary metal chalcogenides ($AgInS_2$, $ZnIn_2S_4$, $AgIn_5S_8$, $CuInS_2$ and $CdIn_2S_4$) have excellent photoelectric properties and strong visible-light absorption (Ganguly et al., 2019a, 2019b, 2021; Ouyang et al., 2021a; Ye et al., 2018), but the visible-light photocatalytic activityof single-component ternary metal chalcogenides is still not satisfactory.

3. Metal sulfide-based Z-scheme photocatalytic system

Metal sulfide-based Z-scheme photocatalytic systems include three different types: all-solid-state (ASS), liquid-phase and direct Z-scheme (Fig. 3). Metal sulfide-based liquid-phase Z-scheme photocatalytic sys- tems consist of metal sulfide, another semiconductor material and electron acceptor/donor (A/D) pairs. The common A/D pairs are NO_3^-/NO_2^-, $[Fe(CN)_6]^{3-/4-}$, IO_3^-/I^-, $[Co(phen)_3]^{3+/2+}$, Fe^{2+}/Fe^{3+} and $[Co(bpy)_3]^{3+/2+}$, which promote electron transfer between metal sulfide and another semiconductor material (Fig. 3a). Higashi et al. fabricated Z-scheme photocatalytic system with CoO_x/TaON photoanodes, metal sulfides and $[Fe(CN)_6]^{3-/4-}$ redox couple (Shirakawa et al., 2017).

Although this liquid-phase Z-scheme photocatalytic system maintains high redox ability, there are still some problems and mistakes: (1) it is subjected to inherent shortcomings such as backward reactions, low photoconversion efficiency, low stability of redox mediator, light-shielding effect, strict application conditions only in the liquid phase and pH sensitivity; (2) The photoexcited electrons in the CB of S2 and holes in the VB of S1 are more prone to react with electron acceptor and donor, respectively. Thus, the transfer of electrons from the CB of S1 to the VB of S2 via the redox couple is unfeasible from thermodynamical view; (3) The thermal motion of redox couple ions is random and fast,and only the redox couple located between an S1 and an S2 are beneficial electron transfer; (4) Since free electrons alone cannot exist in water, the transfer of photogenerated electrons in water medium is unfavorable via the water medium (Xu et al., 2023).

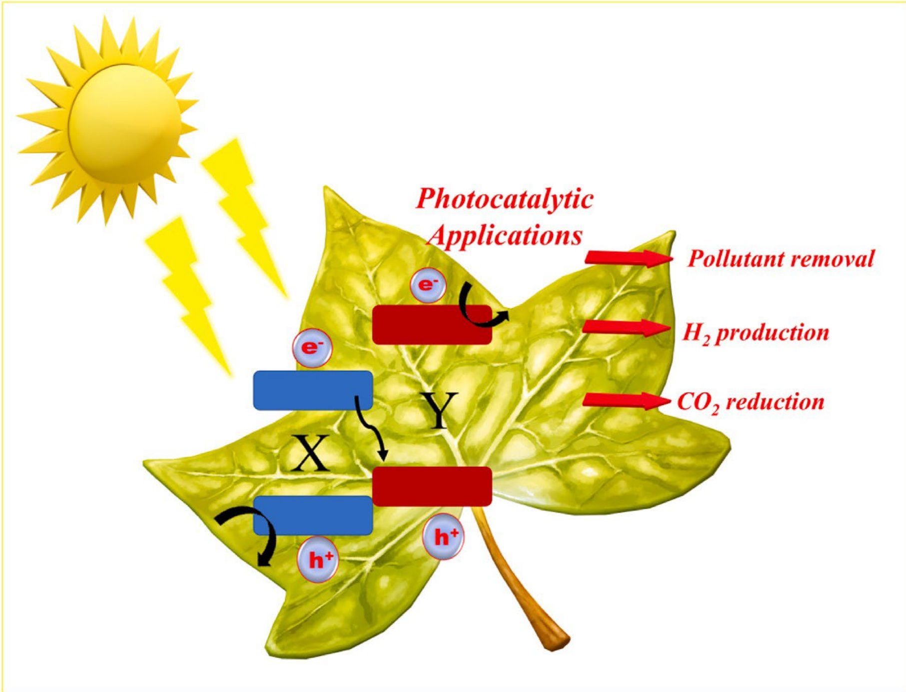

Fig. 2. Graphical representation of metal sulfide-based Z-scheme photocatalysts and applications.

To put up with the defects of liquid-phase Z-scheme photocatalytic systems, the metal sulfide-based ASS Z-scheme photocatalytic system was developed. The redox mediators of metal sulfide-based ASS Z- scheme photocatalytic system are in solid state. The common solid-state electron mediators are Ag, Cu, Au, metallic Bi, graphene oxide (GO) (Min et al., 2014), carbon dots (CDs), reduced graphene oxide (rGO), carbon nanotubes (CNTs) (Wang et al., 2018b; Zheng et al., 2019) and graphene (Gautam et al., 2020). The solid-state electron mediators can generate ohmic contact at the interface of heterojunctions, leading to the minimum connection resistance and short transmission distance. In one of our works, a visible-light-responsive Z-scheme photocatalytic system consisting of Bi_2S_3, BiOBr and rGO as electron mediator was fabricated. This rGO/Bi_2S_3-BiOBr heterojunction displayed effective decomposition of 2-nitrophenol (2NP) and Cr(VI) reduction owing to the reinforcement of electron transfer from Bi_2S_3 to BiOBr via rGO and production of reactive species (Fig. 4) (Li et al., 2019a). Li et al. first prepared sulfur-doped g-C_3N_4 (g-CNS) by calcination at 650 °C, then Au nano- particles were grown on g-CNS surface using chloroauric acid as pre- cursor, and fabricated g-CNS/Au/CdS Z-scheme heterojunction via chemical bath deposition (Li et al., 2015).

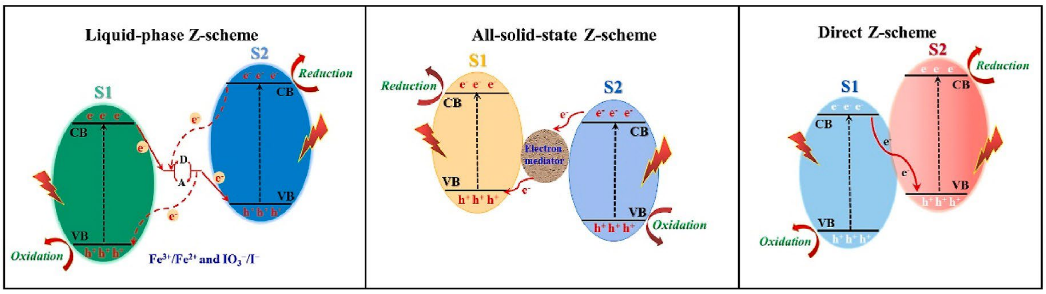

Fig. 3. Charge carrier transfer in different Z-scheme heterojunctions.

The nano-sized Au promoted the face-to-face transport and the annihilation of the e^- of CdS and h^+ of g-CNS. Meanwhile, the e^- on the CB of CdS and the h^+ on the VB of CNS exhibited strong reductive ability and oxidizing performance, respectively. They were participated in the reduction of H^+ to H_2 and oxidation reaction. This g-CNS/Au/CdS showed good visible-light photocatalytic performance and high stability in H_2 evolution and decom- position of dyes due to the prolonged lifetime, boosted redox ability and Z-scheme transfer path of charge carriers. Chai et al. synthesized Z-scheme P-doped $Zn_{0.5}Cd_{0.5}S_{1-x}$/N-doped CNTs/Bi_4NbO_8Cl hetero- junctions which exhibited superior photocatalytic performance in H_2 and O_2 evolution (Ng et al., 2021). The N-doped CNTs with low contact resistance acted as electron mediators and promoted directional electrontransfer. Although the use of solid-state electron mediators inhibits the backward reaction in liquid phase and extends the application in gaseous and solid conditions, there are also some shortcomings with metal sulfide-based ASS Z-scheme heterojunctions: (1) solid-state electron mediators increase the economic cost of metal sulfide-based ASS Z-scheme photocatalyst and reduce light-absorption ability; (2) Due to larger difference in electrode potentials, the electron transfer from theCB of S1 to the VB of S2 is more prone to occur via the solid-state electron mediators, while the charge transfer path from the CB of S2 to the VB of S1 is thermodynamically unfavored; (3) It is difficult toprecisely control the position of solid-state electron mediators between two photocatalysts in synthesis; (4) The band bending is adverse to the interfacial transfer of photogenerated electrons (Wang et al., 2022a). The direct Z-scheme photocatalytic systems are superior to liquid-phase and ASS counterparts due to no loading of electron or hole mediators (Wang et al., 2019b), reduced cost and no shading effect, thusthey have been extensively investigated for various applications. Direct Z-scheme $CuInS_2/Bi_2WO_6$ heterojunction, $CdS/CuInS_2$ nanoplates and ZnS-SnS_2 without electron mediators were reported by us (Lu et al., 2019; Deng et al., 2019; Xia et al., 2020). The interface micro-structuresof these metal-sulfide Z-scheme heterojunctions were regulated by sur- face chemical factors in the growth environment, and effective Z-scheme electron transfer channels were established, leading to directionalcharge transfer without the aid of mediators and the optimal redox capacity. Z-scheme $CuInS_2/Bi_2WO_6$ heterojunctions were synthesized by in-situ growth strategy. The obtained $CuInS_2/Bi_2WO_6$ had close inter- face contact and exhibited outstanding visible-light photocatalytic performance in decomposing organic pollutants, Cr(VI) reduction andpharmaceutical wastewater treatment (Fig. 5) (Lu et al., 2019). More- over, the influence of surface microstructure on pollutant adsorption and interfacial mass transfer, and the influence of pollutant adsorption behavior on the subsequent photocatalytic process were explored. The relationships among the microstructure of Z-scheme $CuInS_2/Bi_2WO_6$ heterojunctions, light absorption performance and active species generation were revealed.

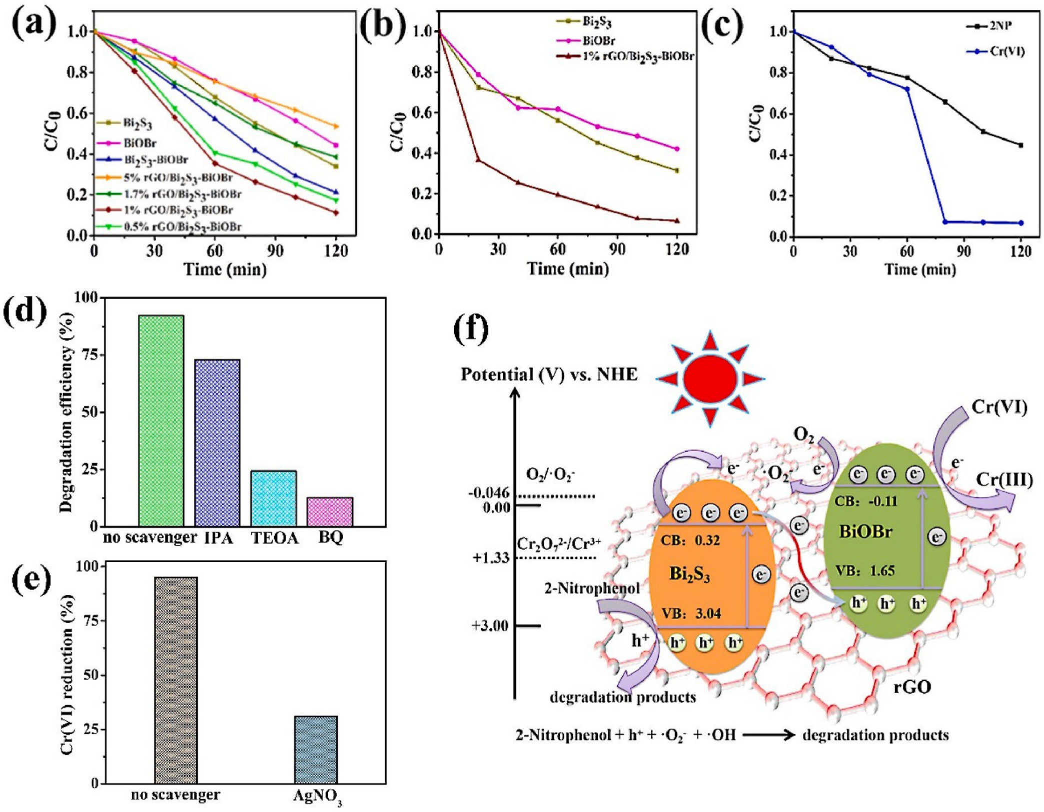

Fig. 4. (a) Photocatalytic decomposition of 2NP solution, (b) Cr(VI) reduction, (c) synchronous photocatalytic redox ability of 1% rGO/Bi_2S_3-BiOBr in 2NP-Cr(VI) mixed solution. (d) Reactive species and (e) electron trapping experiment. (f) Photocatalytic mechanism of 1% rGO/Bi_2S_3-BiOBr. Reproduced with permission from Ref. (65). Copyright 2019, Royal Society of Chemistry.

4. Synthesis methods of metal sulfide-based Z-schemephotocatalysts

The photocatalytic properties of Z-scheme nano-heterojunctions correlate with their composition, size and morphology, thus the controllable synthesis of Z-scheme heterojunctions is of significant importance. In general, the growth of Z-scheme heterojunctions includes two processes: nucleation and growth. However, the nucleationand growth are usually simultaneous, and their thermodynamic and kinetic processes are difficult to control. Therefore, the controllable synthesis of Z-scheme nano-heterojunctions is relatively complex. The type, con- centration and properties of reactants will affect the nucleation and growth of Z-scheme nano-heterojunctions. Moreover, the reaction temperature, reaction time and ambient pressure also have vital influence on the morphology of Z-scheme nano-heterojunctions. This section will briefly introduce several common synthesis methods.

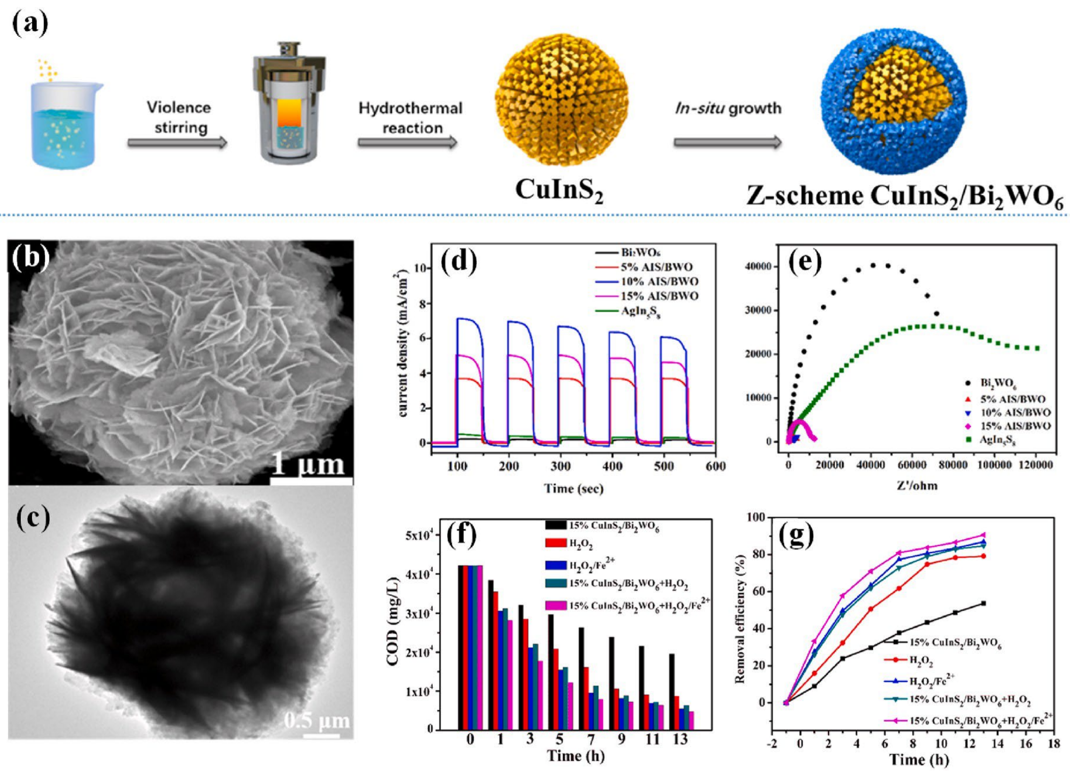

Fig. 5. (a) The synthesis process of Z-scheme $CuInS_2/Bi_2WO_6$; (b) SEM and (c) TEM images of 15% $CuInS_2/Bi_2WO_6$; (d) Photocurrent and (e) EIS; (f) COD changes and (g) COD removal efficiency of pharmaceutical wastewater. Reproduced with permission from Ref. (70). Copyright 2019, Elsevier.

4.1. Hydrothermal method

In the hydrothermal method, inorganic Z-scheme heterojunctions are synthesized from aqueous precursors in a special closed reactor (autoclave) under high temperature and pressure (Ganguly et al., 2019c). Water not only acts as a solvent, but also participates in the reaction. In addition, water is also a medium to transfer pressure. By manipulating reaction temperature, reaction duration, the feed ratios of different metal ions, precursor concentration and sulfur sources, physicochemical properties such as the morphology, crystal structure and size of metal sulfide-based Z-scheme heterojunctions can be controlled, which have important effects on the performance of metal sulfide-based Z-scheme heterojunctions.

There are several reports on the use of hydrothermal techniques as the preferred choice of synthesis. Amongst them, our group fabricated direct Z-scheme $CdS/CuInS_2$ heterojunctions with tight contact interfaces and energy band matching by hydrothermal method, and CdS/ $CuInS_2$ exhibited high photocatalytic activity in decomposing tetracycline and Cr(VI) reduction under visible light (Wang et al., 2019b). Zhang et al. prepared Z-scheme CdS/SnS_2 photocatalyst through a one-step hydrothermal process using $CdSnO_3 \cdot 3H_2O$ as templates and thioacetamide as the sulfur source. The CdS/SnS_2 heterojunctions show superior photocatalytic activity, which is attributable to high light-harvesting, strong adhesion between SnS_2 and CdS, and efficient charge transfer (Zhang et al., 2018). Similarly, other metal sulfide-based Z-scheme heterojunctions such as $CdS/Bi_{12}GeO_{20}$ (Ruan et al., 2019), SnS_2/Ag_3PO_4 (Luo et al., 2016), $CoWO_4/CuNi_2S_4$ (Mao et al., 2020), $ZnIn_2S_4/TiO_2$ (Zhao et al., 2021a), In_2S_3/CeO_2 (Murugalakshmi et al., 2021) and In_2S_3/Ag_2CrO_4 (Luo et al., 2017b) have also been prepared by hydrothermal method. These stable Z-scheme metal sulfide hetero- junctions exhibited extraordinary photocatalytic performance due to intimate contact interfaces and Z-scheme charge transfer. Apart from the use of water as the reaction medium, the multiple roles of water (reac- tant, stabilizer, solvent, etc.) were also explored. The morphologies of these photocatalysts were also pretty interesting.

4.2. Solvothermal method

The operation procedures of solvothermal method are similar to those of hydrothermal method, with organic solvents replacing water. The solvothermal reaction is relatively simple and easy to manipulate. The structure, morphology and crystal phase of Z-scheme nano- heterojunctions can be effectively regulated *via* adjusting the parameters such as temperature, different organic solvents and inorganic ions. The structural and interfacial features of heterojunctions also requiresensible design to promote efficient generation and utilization of pho- to generated charge carriers. The Z-scheme $CdS@ZnIn_2S_4$ hetero- junctions with a chemically bonded interface and hierarchical hollow structures were constructed *via* the growth of $ZnIn_2S_4$ on CdS surface by solvothermal method at low temperature and applied for solar watersplitting to produce H_2 and H_2O_2 (Zhang et al., 2021a).

Different morphologies of photocatalysts provide sensitive active sites for tuning photocatalytic activity. The key strategy for controllable morphology is the sophisticated regulation of reaction conditions for the nucleation and specific growth of photocatalysts by different solvent compositions and various additives. Some studies have elaborated on how different solvents affect the morphology of Z-scheme hetero- junctions. For example, N,N-dimethylformamide, deionized water and ethylene glycol have different effects on the morphology of Z-scheme Bi_2S_3/CdS (Shi et al., 2021). Due to the suitable surface tension and interface energy of ethylene glycol and N,N-dimethylformamide, Bi_2S_3/CdS heterojunctions prepared in N,N-dimethylformamide and ethylene glycol displayed dandelion-like morphology, which was an assembly of hierarchical nanowires, resulting in enhanced interfacial charge separation. The Bi_2S_3/CdS heterojunction synthesized in deion ized water showed a staggered nanowire structure on account of the high surface tension and interface energy of deionized water.

Designing zero-dimensional/three-dimensional (0D/3D) structure of heterojunction is a significant tactic for extending the lifetime of photo generated carriers due to many active sites, short migration distance of photogenerated charges offered by 0D nanomaterials, and large specific surface area (Zhu et al., 2018). Tang et al. constructed Z-scheme 0D/3D CeO_2/$ZnIn_2S_4$ heterojunctions by a solvothermal method (Hao et al., 2021). The 3D flower-shaped spherical structure of $ZnIn_2S_4$ serves as the support, inhibiting the self-aggregation of 0D CeO_2. With a 91% TC degradation efficiency within 2 h, the optimized 10 wt% CeO_2/$ZnIn_2S_4$ heterojunction exhibited satisfactory photocatalytic performance, which was put down to its increased surface area, efficacious separation of photogenerated carriers and powerful redox capacity.

Because of different Fermi energy levels of different semiconductors and interface effect of heterojunction, there are CB (ΔE_{CBO}) and VB offset (ΔE_{VBO}), which could promote the transformation of type I heterojunctions to Z-scheme heterojunctions during solvothermal process. For example, ZnS and SnS_2 are inclined to form type I heterojunction according to their CB and VB positions. In fact, the ΔE_{CBO} and ΔE_{VBO} of ZnS/SnS_2 heterojunction were 0.22 and 1.02 eV, respectively. The band alignment by VB and CB offset tends to construct Z-scheme ZnS/SnS_2 heterojunctions (Fig. 6) (Xia et al., 2020).

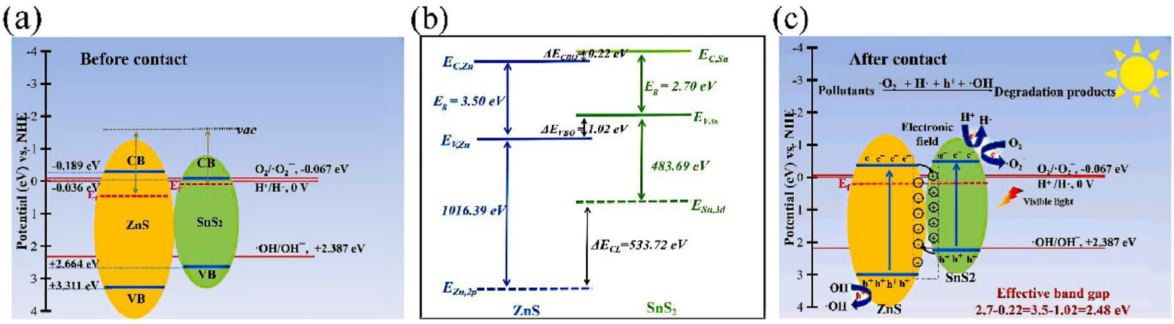

Fig. 6. (a) The band alignment of SnS_2 and ZnS, (b) CB and VB offset and (c) photocatalytic mechanism of Z-scheme ZnS/SnS_2 heterojunctions. Reproduced with permission from Ref. (72). Copyright 2020, Elsevier.

4.3. Multi-step synthesis

Some Z-scheme heterojunctions are challenging to synthesize in one step, but they can be obtained *via* multiple steps. Although the operating procedure of multi-step synthesis is complex, it still has great potential in preparation of Z-scheme heterojunctions. In metal sulfide-based Z-scheme heterojunctions, intimate interface between metal sulfide and other constituents is critical for effective carrier transfer (Ren et al., 2019; Zhang et al., 2020). Growth of one photocatalyst in a precursor solution on the surface of other semi- conductors is an effective strategy to construct Z-scheme hetero- junctions with a tight and stable interface contact, which is in favor of the charge transfer between multiple components (Zeng et al., 2018b). Inspired by this notion, our research group synthesized direct Z-scheme $CuInS_2$/Bi_2WO_6 photocatalysts *via* in-situ growth of Bi_2WO_6 on network-like $CuInS_2$ microspheres with a hydrothermal process (Luet al., 2019). The intimate interface and effective charge transfer via Z-scheme pathways endowed $CuInS_2$/Bi_2WO_6 with excellent photo-catalytic performance. Qiu et al. synthesized Z-scheme SnS_2/BiOBr with visible-light response by an in-situ growth strategy. The significant in- crease in photocatalytic performance of SnS_2/BiOBr was probably attributable to the tight contact interface, leading to fast charge transfer *via* the interface (Qiu et al., 2017b). Z-scheme $BiVO_4$ (040)-Ag@CdS materials were prepared *via* multiple steps. The monoclinic $BiVO_4$ with exposed (040) facets and CdS nanorods were obtained by hydrothermal method, then the deposition of nano-sized Ag on the $BiVO_4$ (040) facets was realized by photoreduction to obtain $BiVO_4$-Ag. The $BiVO_4$ (040)-Ag@CdS was fabricated by the reflux method using $BiVO_4$-Ag and CdS nanorods (Xue et al., 2019). Another example of multi-step synthesis was demonstrated in the assembly of visible-light-responsive Z-scheme CdS/N-CoS_x hetero- junctions (Zhang et al., 2021b). First, CoS_x polyhedrons were synthesized *via* solvothermal process using ZIF-67 as template, and then were handled by N_2 plasma to obtain N-doped CoS_x (N-CoS_x) polyhedrons. The direct Z-scheme CdS/N-CoS_x heterojunction was obtained *via* the growth of CdS on N-CoS_x surface by solvothermal route. The photo- catalytic activities of CdS/N-CoS_x were dependent on the molar ratios of CdS to N-CoS_x and plasma treatment time. The Z-scheme CdS/N-CoS_x with a theoretical molar ratio of 8:1 and 5 min plasma treatment showed the optimal photocatalytic activity with 100% Cr(VI) reduction efficiency, and is highly stable in five cycles. Li et al. synthesized Z-scheme g-C_3N_4/CdS heterojunction *via* chemisorption and self-assembly strategy. The g-C_3N_4/CdS heterostructure showed improved photocatalytic performance in degrading erythromycin and tetracycline, and the photocorrosion of CdS was inhibited effectively *via* the formation of heterostructure with g-C_3N_4 (Li et al., 2019b).

5. Z-scheme photocatalytic mechanism based internal electricfield

The key to increasing photocatalytic efficiency is to boost charge separation (Chen et al., 2021). The internal electric field (IEF) at the interface of Z-scheme photocatalytic system drives charge separation (Xi et al., 2021). Therefore, it is crucial to construct IEF rationally and explore the IEF-based photocatalytic mechanism. Z-scheme heterojunctions can be formed between metal sulfides and other semiconductor materials. Generally speaking, reduction-type photocatalysts have smaller work function (Φ) and higher Fermi level (Fig. 7a), while oxidation-type photocatalysts have larger Φ and lower Fermi level (Fig. 7b). Metal sulfides can be either reduction-type photocatalysts or oxidation-type photocatalysts depending on the Fermi level. When metal sulfide gets in close contact with another semiconductor to produce Z-scheme heterostructure, the e^- in the reduction-type photocatalyst will migrate to the oxidation-type photo- catalyst across the interface until both semiconductors have equal Fermi levels. The reduction-type photocatalyst becomes positively charged, and its band edge bends upward after losing electrons, while the oxidation-type photocatalyst becomes negatively charged after accepting electrons, and its band edge bends downward (Fig. 7c), resulting in an IEF at the interface. In presence of light, the e^- are excited from VB to CB of reduction-type and oxidation-type photocatalysts, and the IEF will drive face-to-face transfer of photogenerated e^- of oxidation-type photocatalyst and h^+ of reduction-type photocatalyst, and accelerate their recombination at the interface with the aid of Coulomb interaction and band edge bending (Fig. 7). Meanwhile, the e^- in CB of reduction-type photocatalyst and h^+ in VB of oxidation-type photocatalyst are spatially separated, leading to strong redox ability (Zhang et al., 2019a). This photocatalytic mechanism based on IEF and Z-scheme path is good for decomposition of organic pollutants, H_2 evolution and CO_2 reduction.

The existence of an IEF and interfacial charge migration direction are important for exploring the underlying mechanism of Z-scheme photo- catalysis. Atomic force microscope (AFM), Kelvin probe force microscopy (KPFM) equipped with surface photovoltage technique can image the gathering of photogenerated e^- and h^+ at two sides of the interface. Thus, the localized charge separation can be visualized, and these two inverse charge transfer processes can be differentiated directly (Fig. 8) (Lin et al., 2021). Moreover, the trapping experiment of reactive species, density functional theory (DFT) calculation, time-resolved spectroscopy understanding the transfer pathway of photogenerated carriers through the interface of junction and photocatalytic mechanism of Z-scheme heterojunctions (Li et al., 2021c; Lee et al., 2019).

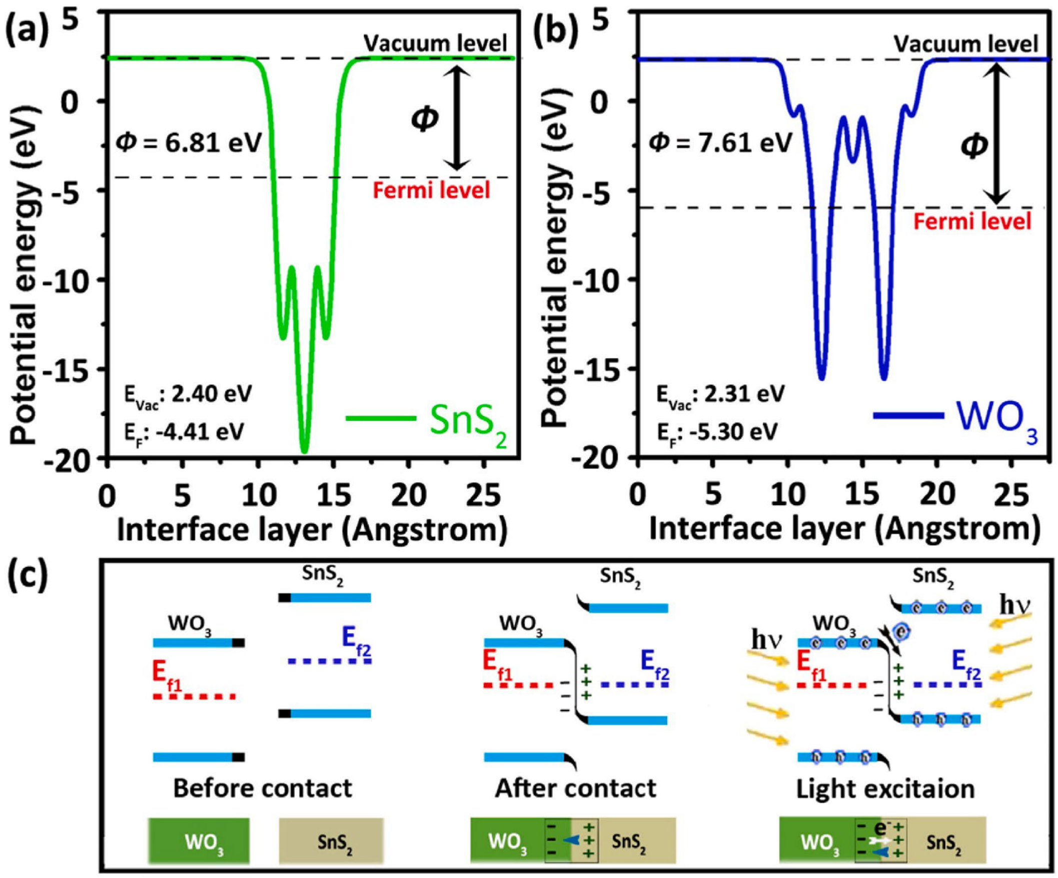

Fig. 7. The Φ of SnS_2 (a) and WO_3 (b); Band structure of SnS_2 and WO_3, and Z-scheme carrier transfer (c). Reproduced with permission from Ref. (94). Copyright 2019, Elsevier.

Our group has fabricated Z-scheme $AgIn_5S_8/ZnO$ nanocomposites, which exhibited outstanding photocatalytic activities in decomposing pharmaceutical pollutants. Moreover, the Φ values of ZnO and $AgIn_5S_8$ were obtained from VB XPS and calculation (Xu et al., 2022b), and the IEF in $AgIn_5S_8/ZnO$ was verified using AFM equipped with KPFM. The Z-scheme path of charge transfer in $AgIn_5S_8/ZnO$ was driven by IEF, which was shown in Fig. 9. To further confirm the Z-scheme path of charge transfer, the main active species in photocatalysis can be analyzed by radical trapping experiments. Tert-butyl alcohol (TBA), coumarin and isopropanol (IPA) are usually used as scavengers of ·OH radicals. The p-benzoquinone (BQ) and N_2 atmosphere are commonly utilized as the scavengers of O_2^-. EDTA, triethanolamine (TEOA) and ammonium oxalate are extensively applied as the scavengers of h^+ (He et al., 2015; Yuan et al., 2017a; Li et al., 2018). Electron spin resonance (ESR) spectroscopy is also extensively utilized to detect $·O_2^-$ and ·OH radicals using 5,5-dime- thyl-1-pyrroline N-oxide (DMPO) as spin trap (Fig. 10). The DMPO-$·O_2^-$ and DMPO- OH peaks in ESR spectra authenticate the existence of O_2^- and OH radicals (Jiang et al., 2020). According to VB and CB of reduction-type photocatalyst and oxidation-type photocatalyst, active species, and the redox potentials for the generation of OH and O_2^- radicals, and the existence of IEF, the underlying Z-scheme photocatalytic mechanism can be inferred.

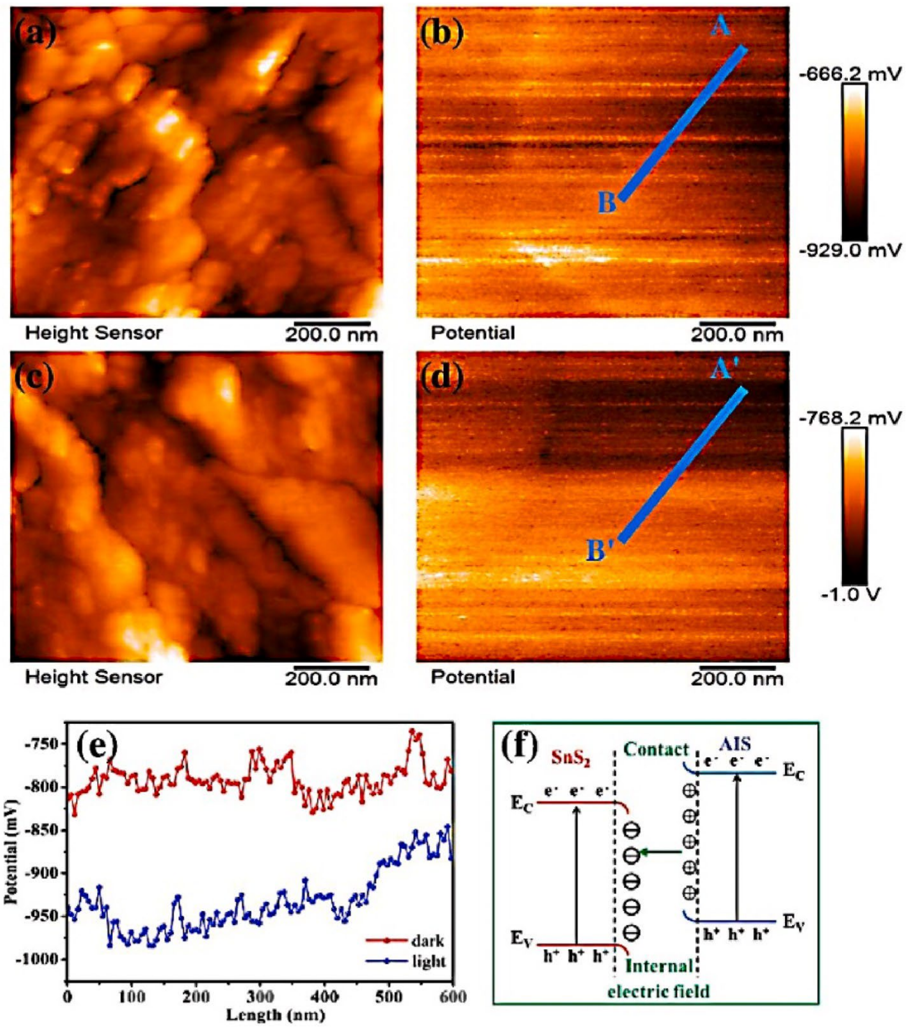

Fig. 8. AFM (a) and KPFM (b) of AIS (0.8%)/SnS_2 in the dark. AFM (c) and KPFM (d) of AIS (0.8%)/SnS_2 under visible light. (e) Average surface potential and (f) Z-scheme charge transfer. Reproduced with permission from Ref. (Lin et al., 2021). Copyright 2021, Elsevier.

6. Application of metal sulfide-based Z-scheme photocatalysts

6.1. Photocatalytic decomposition of organic pollutants

The decomposition efficiency of organic contaminants is extensively applied to estimate the photocatalytic activity of Z-scheme photo- catalysts and the transformation degree of parent pollutants. Table 1 shows some Z-scheme sulfide-based heterojunctions for degradation of organic pollutants. However, the degradation efficiency of organic pollutants reflects neither the content of organic intermediate products in aqueous solutions nor practical application potential. The potential application of metal sulfide-based Z-scheme photocatalysis in environ- mental restoration has been widely investigated. For example, Z-scheme $AgIn_5S_8/ZnO$ was used to decontaminate organic contaminants and enhance biodegradability of real wastewater. Total organic carbon(TOC) and chemical oxygen demand (COD) can assess the content of organic pollutants in wastewater. Moreover, the biodegradability parameters such as carbon oxidation state (COS) and average oxidationstate (AOS) based on COD and TOC data can be obtained according to the following equations:

$$COS = 4 - 1.5 \times \frac{COD}{TOC_0} \quad (1)$$

$$AOS = 4 - 1.5 \times \frac{COD}{TOC} \quad (2)$$

where TOC_0 represents initial TOC concentration, *TOC* and *COD* are corresponding values (mg/L) of wastewater at different irradiation time. The increase of AOS and COS values with irradiation time indicates that photocatalysis can enhance the biodegradability of wastewater. The increasing AOS and COS values from 0.42 to 1.35 and 2.94 in our previous studies confirm that the photocatalysis of Z-scheme $AgIn_5S_8/ZnO$ heterojunctions can greatly enhance the biodegradability of pharmaceutical wastewater (Fig. 11) (Xu et al., 2022b).

Degradation efficiency of organic pollutants, COD, TOC, AOS and COS values cannot give important information on toxic groups of organic pollutants and the change of biological toxicity during photo-catalytic process. Therefore, it is of vital importance to investigate the degradation path of organic pollutants and the toxicity of intermediates. In some studies, the decomposition and mineralization paths of organic pollutants by metal sulfide-based Z-scheme heterojunctions were studied by analyzing degradation intermediates at different time using high performance liquid chromatography-mass spectrometry (HPLC-MS) (Xia et al., 2020). The growth of *Escherichia coli* in culture medium containing degradation solutions at different degradation stages wereanalyzed qualitatively and quantitatively to evaluate the toxicity of parent pollutants and their intermediates (Fig. 12). *D. magna* is also frequently utilized for toxicity evaluation of intermediate products during photocatalytic process due to its rapid reproduction, short life cycle, easy cultivation and sensitivity to toxic substances (Li et al., 2020a). Moreover, the ecological structure activity relationships (ECO- SAR) model can predict the toxicity of organic pollutants and their degradation intermediates (Li et al., 2020a; Lv et al., 2022). By detecting comprehensive toxicity of degradation intermediates at different degradation stages, the non-toxic degradation pathway of typical anti- biotics can be regulated by changing the composition, microstructure and application conditions of the catalyst.

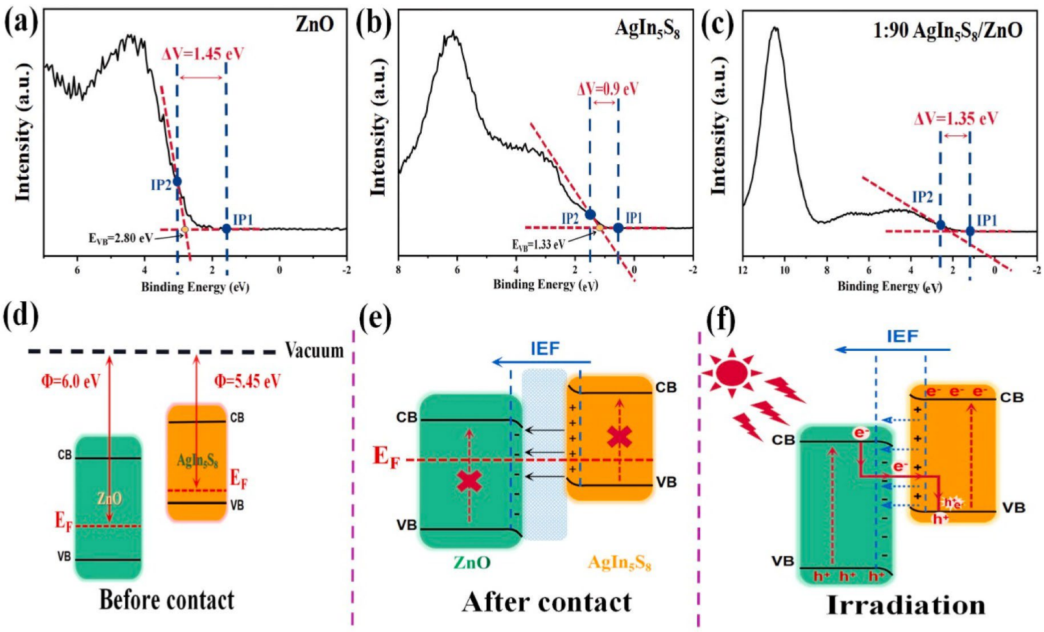

Fig. 9. (a) VB XPS of ZnO, (b) $AgIn_5S_8$ and (c) $AgIn_5S_8/ZnO$; the band structure of ZnO and $AgIn_5S_8$ before (d) and after contact; (e) Z-scheme charge transfer in $AgIn_5S_8/ZnO$ (f). Reproduced with permission from Ref. (Xu et al., 2022b). Copyright 2022, Elsevier.

6.2. Photocatalytic H_2 production

H_2 is supposed as ideal alternative energy on account of its high calorific value (122 kJ/mol), zero carbon emission, environmental friendliness and storability (Li et al., 2021d, 2022a). At present, H_2 is mainly produced from natural gas via the reforming of steam methane, and the obtained H_2 is still a product of fossil instead of renewable energy. The key issues for the preparation and application of H_2 fuel are the development of green and effective H_2 production methods, which are not dependent on the use of fossil fuels (Yuan et al., 2018). Photo- catalytic H_2 production shows huge potential in alleviation of energy crisis by conversion of solar energy to H_2(Li et al., 2022b; Zhou et al., 2022). The reaction of photocatalytic water splitting includes O_2 evolution and H_2 evolution. Since the first report on water splitting for H_2 production by TiO_2 in 1972, various metal sulfide semiconductors have been utilized for photocatalytic H_2 production (Lai et al., 2012). Un- fortunately, not all the single-component metal sulfide semiconductors can meet the fundamental requests for photocatalytic H_2 production: more positive VB than H_2O/O_2 potential (1.23 V) and more negative CB than H^+/H_2 potential (0 V). The E_g of semiconductors should be larger than 1.23 eV (Zhang et al., 2022; Li et al., 2022c). Moreover, the high recombination rate of charge carriers of single-component metal sulfide semiconductors is still a limiting factor for the application (Guo et al., 2023). Thus, the construction of sulfide-based Z-scheme heterojunctions is a fantastic tactic to surmount the shortcomings of single-component metal sulfide semiconductors, which is beneficial to photocatalytic H_2 production.

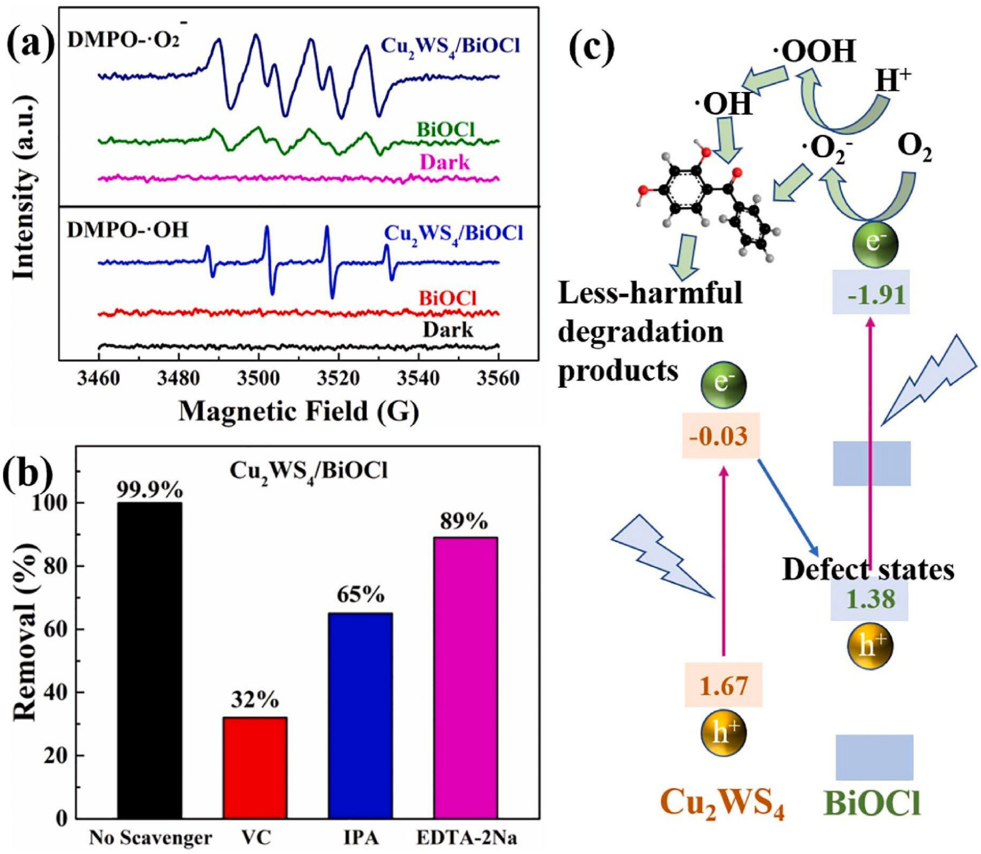

Fig. 10. ESR spectra of $\cdot$OH and $\cdot O_2^-$ (a), trapping of active species (b), and photocatalytic mechanism of Cu_2WS_4/BiOCl (c). Reproduced with permission from Ref. (Jiang et al., 2020). Copyright 2020, Elsevier.

The exploitation of noble-metal-free cocatalysts in Z-scheme systems for solar H_2 production has attracted huge interest. Yu et al. fabricated a Z-scheme photocatalytic system using $Co_3O_4/BiVO_4$, MoS_2/CdS and $[Co(bpy)_3]^{3+}/[Co(bpy)_3]^{2+}$ redox couple as O_2 evolution photocatalyst, H_2 evolution photocatalyst and electron mediator, respectively (Yuan et al., 2017b). The highest O_2 and H_2 evolution rates are 14.5 and 7.1 mmol h^{-1} in this Z-scheme photocatalytic system with 4 wt% MoS_2/CdS and 1.5 wt% $Co_3O_4/BiVO_4$ under visible-light exposure, respectively. The superior H_2 evolution efficiency and high stability of this Z-scheme system indicate its good potential for solar H_2 generation.

The inhibition of backward reactions by shuttle redox mediators isstill challenging in constructing liquid-phase Z-scheme photocatalytic systems for water splitting, thus the development of Z-scheme photo- catalytic systems without shuttle redox mediators is preferred. Xie et al. synthesized Z-scheme CdS/WO_3 junction for H_2 production (Zhang et al., 2014). The Z-scheme 20 wt % CdS/WO_3 photocatalyst showed high photocatalytic activity with H_2 release rate of 369 μmol g^{-1} h^{-1}, which is about 5 times that of CdS in presence of lactic acid (Fig. 13a). The introduction of noble metal Pt in Z-scheme CdS/WO_3 can further improve the charge transportation between the interface of CdS and WO_3, leading to dramatic H_2 release rates of 2900 μmol g^{-1} h^{-1} under irradiation of visible light (Fig. 13b). The photocatalytic mechanism of CdS/WO_3 for H_2 production was shown in Fig 13c. Because of higher Φ of WO_3 than CdS, the e^- transferred from CdS to WO_3 until reaching the same Φ after the contact of CdS with WO_3. With bands bending, IEF is formed at the junction interface. The potential barrier will be set up by the CB bending of CdS. Under light exposure, the e^- was excited from the VB of WO_3 and CdS to their CB. The internal electricfield drove the transfer and recombination of photogenerated e^- in CB of WO_3 with h^+ in VB of CdS (Fig. 13). Meanwhile, more e^- in CB of CdS were involved in reducing H^+ and H_2 evolution.

Zhang et al. prepared direct Z-scheme CdS/Co_9S_8 heterojunction byembedding Co_9S_8 cubes with CdS quantum dots (QDs) for photocatalytic water splitting (Lv et al., 2022). The H_2 evolution rate on Z-scheme CdS/Co_9S_8 heterojunction is 9.1 and 134-fold higher than that of CdS

Table 1
Z-scheme sulfide-based heterojunctions for degradation of organic pollutants.

Photocatalyst/Dosage	Synthesis	Pollutant/Concentration	Light Spectra	Intensity (W)	Time (min)	Efficiency (%)	Ref.
$ZnIn_2S_4@MoO_3$ (150 mg/L)	Hydrothermal method	Tetracycline (30 mg/L)	Xe lamp	420	120	94.5	Ouyang et al. (2021b)
$CdS/CQDs/g-C_3N_4$ (1000 mg/L)	Calcination method	Rhodamine B (10 mg/L)	Xe lamp	300	90	98	Feng et al. (2020)
Ag/NH_2-MIL-125(Ti)/CdS (500 mg/L)	Chemical bath deposition method	Ketoprofen (10 mg/L)	Xe lamp	350	180	94.2	Zheng et al. (2021)
$BiVO_4/Ag/CdS$ (400 mg/L)	Chemical deposition method	Norfloxacin (19.78 mg/L)	Xe lamp	350	90	98.33	Gao et al. (2022)
$Ag-C_3N_4/SnS_2$ (400 mg/L)	Hydrothermal method	Tetracycline (15 mg/L)	Xe lamp	500	150	94.9	Zhao et al. (2021b)
O-CN/CdS (700 mg/L)	Solvothermal method	2-chlorophenol (10 ppm)	Xe lamp	300	60	100	Zhang et al. (2023)
$Ag_3PO_4/1T@2H-MoS_2$ (200 mg/L)	Hydrothermal method	Tetracycline (10 mg/L)	Xe lamp	500	40	98.9	Hua et al. (2023)
$MoS_2/Ag-ZnFe_2O_4$ (800 mg/L)	Hydrothermal method	Tetracycline (10 mg/L)	Xe lamp	300	60	94.8	Zhu et al. (2023)
$BC/2ZIS/WO_3$ (100 mg/L)	Facile hydrothermal method	Rhodamine B (95 mg/L)	Xe lamp	300	120	99	Cheng et al. (2022)
In_2S_3/Ti_3C_2 (600 mg/L)	Hydrothermal synthesis	Sulfamethoxazole (10 mg/L)	Xe lamp	300	150	98	Saravanakumar et al. (2023)

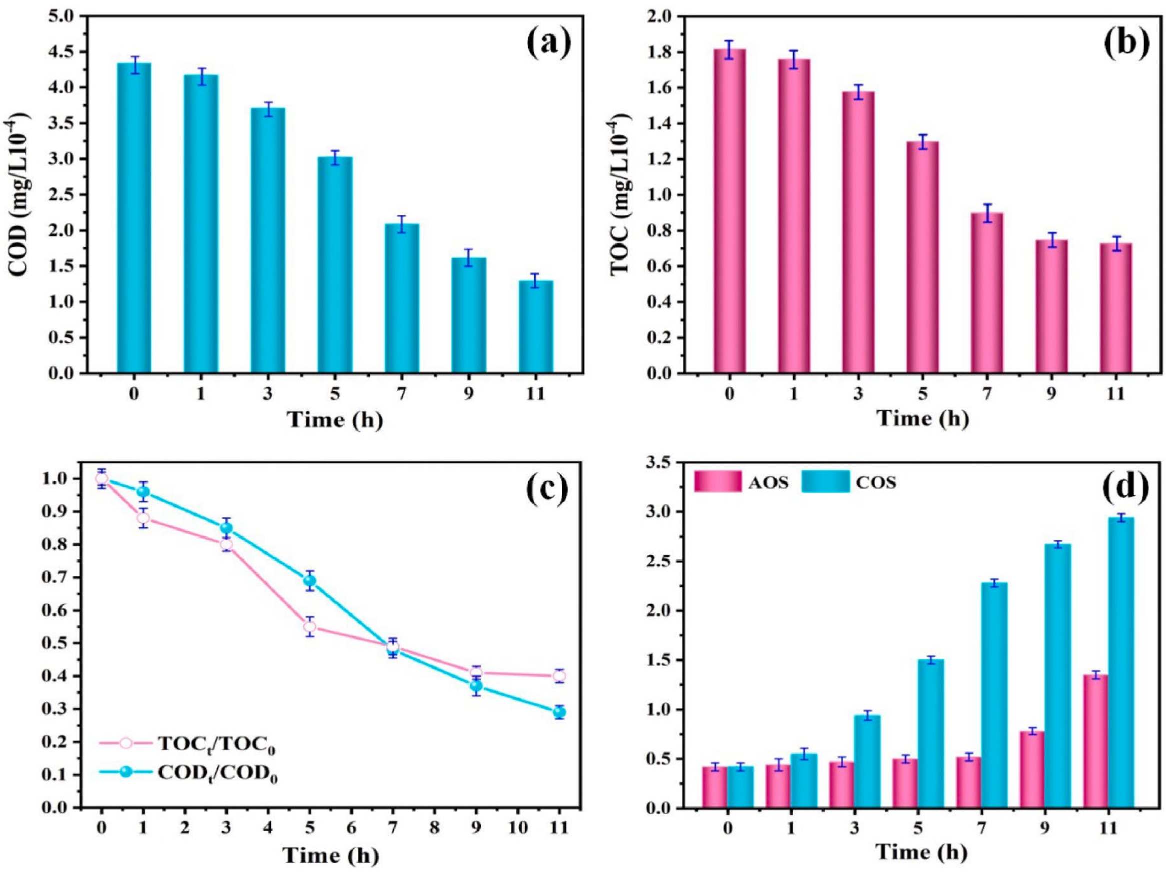

Fig. 11. COD (a) and TOC values (b) of real wastewater during the photocatalytic process; COD and TOC removal efficiency (c), real-time change of AOS and COS (d). Reproduced with permission from Ref. (Xu et al., 2022b). Copyright 2022, Elsevier.

QDs and Co_9S_8 under illumination of simulated sunlight, respectively. The outstanding photocatalytic performance of Z-scheme CdS/Co_9S_8 was attributable to multiple reflections and lighting, and efficacious separation of photoexcited charge carriers. Li et al. synthesized a Z-scheme heterojunction consisting of sulfur vacancy-rich $ZnIn_2S_4$ and $MoSe_2$ (S_v-$ZnIn_2S_4$/$MoSe_2$) for photocatalytic H_2 release under monochromatic light at 420 nm. The optimized Z-scheme S_v $ZnIn_2S_4$/$MoSe_2$ heterojunction exhibits good performance with an H_2 release rate of63.21 mmol g^{-1} h^{-1}, which is 18.8 times of bare $ZnIn_2S_4$. The enhanced activity of Z-scheme S_v-$ZnIn_2S_4$/$MoSe_2$ for H_2 release is attributable to the synergism of interfacial Mo-S bond, S vacancies and internal electric field. The interfacial Mo-S bonds act as direct channels of charge transfer between $MoSe_2$ and S_v-$ZnIn_2S_4$. The S vacancies can promote the separation of photocarriers and enhance optical absorption. The internal electric field drives the charge transfer via S-scheme path between $MoSe_2$ and S_v-$ZnIn_2S_4$ (Fig. 14) (Wang et al., 2021a).

Table 2
Z-scheme sulfide-based heterojunctions for hydrogen production.

Composite type	Sacrificial	Light source (wavelength)	H_2 evolution rate (μmol h^{-1} g^{-1})	AQY	(%)
	Stability (h)	Ref. $NiTiO_3/Cd_{0.5}Zn_{0.5}S$	Na_2S/Na_2SO_3	NA	1058
	34 (420 nm)	>12	Li et al. (2021e)		
CdS-Au	Na_2S/Na_2SO_3	300W Xe lamp (λ > 420 nm)	102.9	9.6 (420 nm)	>44
	Liang et al. (2018a)	g-C_3N_4/CdS	Na_2S/Na_2SO_3	300W Xe lamp (λ > 420 nm)	
	1809.07	2.79 (420 nm)	>40	Wang et al. (2021b)	CdS@WO_3
	lactic acid	300W Xe lamp (λ > 450 nm)	736.89	1.72 (450 nm)	>25
	Zhang et al. (2019b)	CoS/CdS	lactic acid	300W Xe lamp (λ > 400 nm)	
	39290	14.5 (400 nm)	>16	Li et al. (2022e)	

*NA, not available.

The simultaneous production of value-added molecules (carboxylic acids, ethanol, etc.) and energy generation or wastewater remediation using $ZnIn_2S_4$ in a single redox cycle is an excellent strategy (Pillai and Kumaravel, 2021). Li et *al* designed Z-scheme $ZnIn_2S_4$/WO_3 hetero- junctions with intimate interfacial contact via facile solvothermal as- sembly of WO_3 nanorods with $ZnIn_2S_4$ nanosheets, and demonstrated an excellent strategy of coupling organic synthesis and H_2 generation in a single redox cycle using a Z-scheme $ZnIn_2S_4$/WO_3 heterojunction (Li et al., 2022d). The fabrication of Z-scheme $ZnIn_2S_4$/WO_3 hetero- junctions promotes the effective charge separation (Fig. 15a). The photogenerated e^- and h^+ are spatially separated by their

redox sites, and the band edge potentials can be manipulated to attain strong redox abilities for the production of targeted organic products. The optimized $ZnIn_2S_4$/WO_3 heterojunctions possessed the highest photocatalytic performance with 174 μmol benzaldehyde production and 214 μmol H_2 evolution. Integrating H_2 production or wastewater remediation with the generation of organic products is a major advance (Fig. 15b) (Chauhan et al., 2021). The large-scale H_2 production is the ultimate goal of research. Some research teams have developed a prototype reactor which is able to generate massive H_2 under natural sunlight (around 6.1 L in 8 h) as shown in Fig. 15c (https://dst.gov.in/large-s-cale-reactor-developed-cost-effective-production-hy- drogen-using-sunlight-and-water). Various Z-scheme sulfide-basedheterojunctions for H_2 production are shown in Table 2.

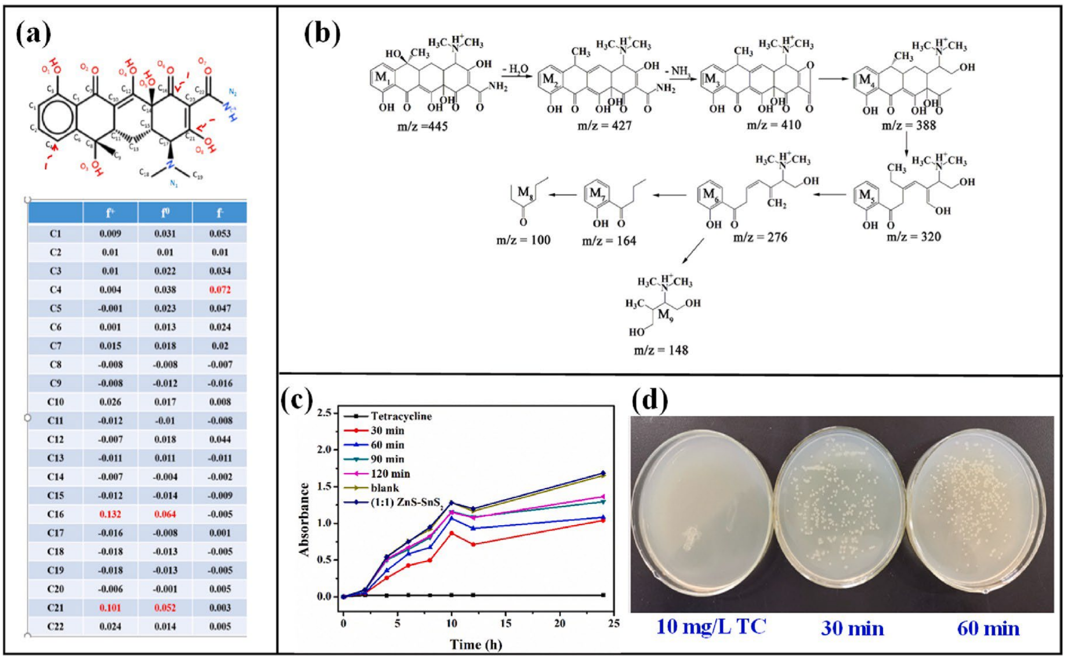

Fig. 12. (a) Fukui index of tetracycline, (b) degradation path, (c) growth curves of *Escherichia coli* in liquid medium (d) formation of *Escherichia coli* colony in solid medium containing degradation solution of tetracycline at different time. Reproduced with permission from Ref. (Xia et al., 2020). Copyright 2020, Elsevier.

6.3. Photocatalytic CO_2 reduction

The large-scale use of fossil fuels and the continuous increase of CO_2 emission from human activities have led to energy crises and global warming (Zeng et al., 2020). Enlightened by the natural photosynthesis which converts CO_2 and H_2O to O_2 and hydrocarbons under the sunlight, the transformation of CO_2 to valuable carbonaceous chemicals such as CH_4, HCOOH, CH_3OH and ethanol (CH_3CH_2OH) by photocatalytic technology has been considered as one of the most attractive way to deal with carbon emission and energy crises (Xu et al., 2019; Pan et al., 2017). Since the first report on the UV photoreduction of CO_2 to organic compounds, TiO_2, CdS, Fe_2O_3, Cu_2O and other semiconductor materials have been used for photocatalytic CO_2 reduction to HCOOH, CO, CH_3OH, HCHO and CH_4 (Zhao et al., 2021c). However, CO_2 reduction efficiency of single-component semiconductors is relatively low in virtue of highly stable CO_2 molecules and speedy recombination of photo-generated carriers (Yoshino et al., 2022). The photocatalytic CO_2 reduction includes CO_2 reduction and H_2O oxidation, which involves the fracture of C-O bonds and formation of C-H bonds (Ran et al., 2018). The above two half-reactions are full of challenges because of their high bond energy. Huge endeavors have been devoted to enhancing energy conversion efficiency and extending optical absorption range. However, the photocatalytic CO_2 reduction efficiency and reaction selectivity of high-value chemicals remain low (Li et al., 2020b). Thus, the development of efficient photocatalysts with high stability is of great significance for CO_2 reduction. Metal sulfide Z-scheme heterojunctions show strong redox capacity, effective transfer of photogenerated charge carriers, wide spectral response and high stability, thus many studies have concentrated on the possible application of metal sulfide Z-scheme heterojunctions in photocatalytic CO_2 reduction (Liang et al., 2018b; Ma et al., 2021). Yu et al. synthesized direct Z-scheme CdS-WO_3 heterojunctions by direct growth of CdS on WO_3 spheres for converting CO_2 to CH_4 (Jin et al., 2015). The higher CO_2 reduction efficiency of CdS-WO_3 under the exposure of visible light than that of WO_3 and CdS was put down toenhanced adsorption for CO_2 molecules, efficient spatial separation and Z-scheme transfer of photogenerated charge carriers. Zou's research group constructed a Z-scheme WO_3/Au/In_2S_3 photocatalytic system via a step-by-step vapor deposition process for CO_2 reduction (Li et al., 2016c). The WO_3/Au/In_2S_3 shows much higher photocatalytic activity than WO_3/In_2S_3 in conversion of CO_2 to CH_4which result from the positive role of Au nanoparticles in promoting oriented migration of e^- from CB of WO_3 to VB of In_2S_3 across theinterface. The differences between the SPV images of WO_3/Au/In_2S_3 and WO_3/In_2S_3 under light and in the dark also confirm that Au nano-particles have important impact on charge transfer between In_2S_3 and WO_3 (Fig. 16).

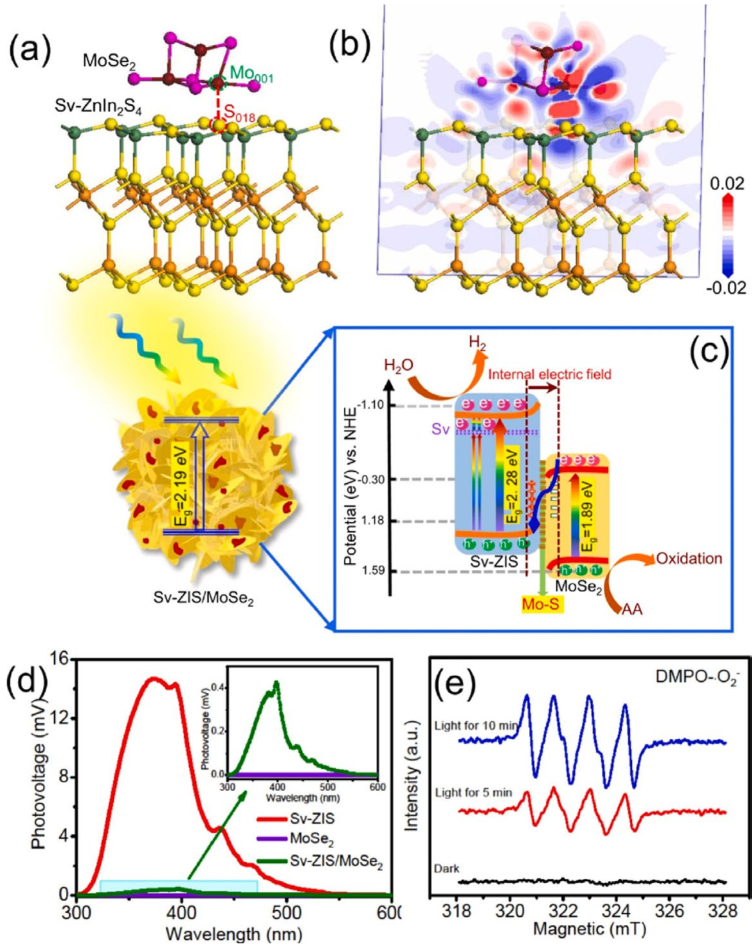

Fig. 14. (a) The structure of S_v-$ZnIn_2S_4$/$MoSe_2$, (b) side view of charge density difference, (c) photocatalytic mechanism of S_v-$ZnIn_2S_4$/$MoSe_2$; (d) Surface photo- voltage of $MoSe_2$, S_v-$ZnIn_2S_4$ and S_v-$ZnIn_2S_4$/$MoSe_2$, (e) EPR spectra of DMPO-$\cdot O_2^-$. Reproduced with permission from Ref. (Wang et al., 2021a), Copyright 2021, Springer Nature.

The photogenerated e^- in the CB of In_2S_3 and h^+ in the VB of WO_3 have strongredox ability, which can facilitate the generation of CH_4. Some Z-scheme sulfide-based heterojunctions for CO_2 reduction are shown in Table 3.

Yan et al. proved the Z-scheme heterostructures of B-doped g-C_3N_4/SnS_2 by DFT calculations on charge density and work function (Wang et al., 2018c). The stronger light absorption and narrower E_g of Z-scheme g-C_3N_4/SnS_2 heterostructures than those of g-C_3N_4 can improve photocatalytic performance. The photocatalytic activity was assessed by calculating the free energy for each reaction step of CO_2reduction, and the products of CO_2 reduction were predicted as CH_3OH and CH_4. The rate-determining step and optimal path for CO_2 reduction were also obtained from calculations.
Although there is some progress on CO_2 photocatalytic reduction by Z-scheme heterojunctions, it is still at the initial research stage, and there are still many unsolved scientific problems. By far, the products of photocatalytic CO_2 reduction by Z-scheme heterojunctions are mainly C1 (CO, CH_4), and it is difficult to generate C2 and C3 products with high yield and high selectivity (Sun et al., 2018b). In the future, it is necessary to combine theoretical calculation with in-situ ESR, in-situ Fourier transform infrared spectroscopy (FTIR) and other advanced characterization methods to explore the reaction mechanism deeply. The kinetics and thermodynamics of the transformation to C2 and C2 products after the formation of initial C-C bond deserve more attention, and the selectivity of products should be rationally regulated through interface modification and the use of catalytic additives (Albero et al., 2020). Moreover, the charge transfer path in Z-scheme heterojunction is notfully clear, and the deep correlation between charge transfer and CO_2 reduction should be revealed. The dependence of solvation effect, activation energy barrier and energy gap on chemical potential is usually ignored in the construction of reaction path by conventional DFT calculation. The path of reduction products is unclear, and evaluation ofreaction activity is still inaccurate.

Table 3
Recent representative studies on the use of metal sulfide-based Z-scheme heterojunctions for CO_2 reduction.

Photocatalyst	Sacrificial	Light source (wavelength)	Product evolution rate (μmol h^{-1} g^{-1})	AQY (%)	Stability (h)	Ref.
$Bi_2O_{2.33}$–CdS	Na_2S/ Na_2SO_3	300W Xe lamp (λ > 420 nm)	CO:2.9	34 (420 nm)	>16	Wang et al. (2022b)
$Bi_{19}S_{27}Br_3$/g-C_3N_4	Not add	300W Xe lamp (λ > 420 nm)	CO: 12.87	NA	>24	Zhao et al. (2022)
$BiVO_4$/Bi_2S_3	Na_2S/ Na_2SO_3	300W Xe lamp (λ > 420 nm)	CH_3OH: 12.5 ± 1.25	NA	>24	Wang et al. (2022c)
$Zn_xCd_{1-x}S$/Au@g-C_3N_4	Glucose	300W Xe lamp (λ > 420 nm)	CH_3OH: 1.31	NA	>12	Madhusudan et al. (2021)
WO_3-TiO_2/Cu_2ZnSnS_4	NA	400W Xe lamp (λ > 420 nm)	CO: 15.37 CH_4:1.69	CO: 0.36 CH_4:0.16	>20	Raza et al. (2020)

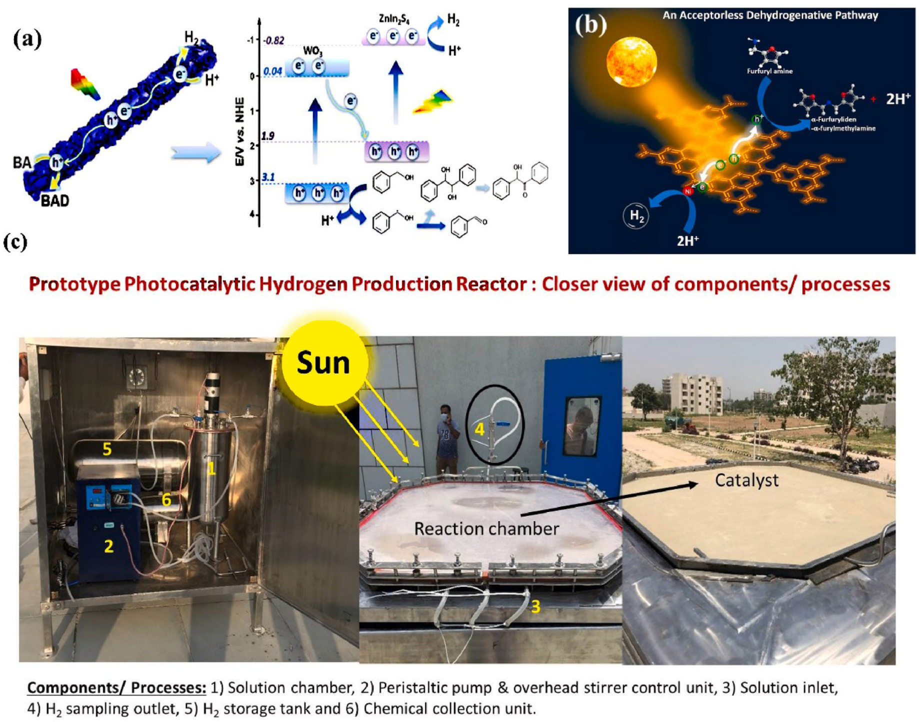

Fig. 15. (a) Photocatalytic mechanism of WO_3/$ZnIn_2S_4$ for synchronous oxidation of benzyl alcohol and H_2 generation; Reproduced with permission of Ref. (Li et al., 2022d). Copyright 2021, American Chemical Society. (b) valorization of furfuryl amine to corresponding imine integrated with H_2 generation; Reproduced with permission of Ref. (Chauhan et al., 2021). Copyright 2021, Elsevier. (c) Large scale pilot plant for H_2 generation.

7. Conclusion and future perspectives

Photocatalysis has promising prospects for solving environmental pollution and energy crisis. As an important type of catalysts, metal sulfide-based Z-scheme heterojunctions have the properties of high visible-light utilization, easy separation of photogenerated carriers and strong redox capacity. In this review, the properties of metal sulfide, the energy band arrangement and charge transfer rules of metal sulfide- based Z-scheme heterojunctions, the characteristics, advantages and shortcomings of different Z-scheme metal sulfide heterojunctions, thesynthesis methods, IEF-based photocatalytic mechanism, and the application in decomposition of organic contaminants, H_2 evolution and CO_2 reduction were discussed.

Although metal sulfide-based Z-scheme heterojunctions have many unique advantages and several encouraging progresses have been achieved, there are still some challenges: (1) Various techniques have been explored for the lab-scale synthesis of metal sulfide-based Z- scheme heterojunctions, however, they may not be applicable in large- scale production. The low-effective light utilization and low light quantum efficiency are still the bottlenecks for practical application. (2) Although the redox ability and stability of metal sulfide-based Z-scheme heterojunctions were enhanced, and decomposition efficiency of organic pollutants was increased, organic pollutants cannot be completely mineralized. Some stable and more toxic intermediates are usually produced. Thus, how to regulate the degradation pathway of organic pollutants, in particular, how to preferentially destroy the toxic groups of organic pollutants, is an imperative problem. (3) The production level of the chemicals from photocatalytic CO_2 production and H_2 production are still in the range of μmol g^{-1} h^{-1}, which is far from large-scale production. Moreover, the photo-corrosion, the aggregation of catalysts and the poisoning by the strongly adsorbed species are major causes for deactivation of catalysts, which could obstruct the reaction continuity and increase the production costs of CO_2 and H_2.

Inspired by the present progress and challenges in this research area, some major questions that need further investigation and clarificationare proposed as follows: (1) the electron-transfer path of Z-scheme heterojunctions was wrong, and S-scheme heterojunction was proposed to overcome the shortcomings of mechanism of Z-scheme hetero- junctions. In S-scheme heterojunction, the spontaneous diffusion of electrons in the reduction photocatalyst to oxidation photocatalyst will create electron depletion layer near the interface of reduction photo-catalyst and electron accumulation layer near the interface of oxidation photocatalyst, leading to the formation of internal electric field between negatively-charged oxidation photocatalyst and positively-charged reduction photocatalyst. This internal electric field promotes the trans- fer of photogenerated electrons from oxidation photocatalyst to reduction photocatalyst. Meanwhile, the upward and downward band bending of reduced and oxidized photocatalysts promote the interfacial recombination of photogenerated electrons in the CB of oxidized photocatalyst and holes in the VB of reduced photocatalyst due to the Coulomb force. This charge transfer path endows efficient separation of the photogenerated carriers and strong redox ability of S-scheme heterojunction (Xu et al., 2020; Wageh et al., 2021). (2) Engineering application is an important direction of our efforts. Industrialized manufacturing equipment for the large-scale production of metal sulfide-based Z-scheme heterojunctions with extraordinary photo- catalytic performance, high stability and excellent durability should be introduced, and the fixation of photocatalysts on proper supports and the fabrication of large-scale photocatalytic reactors should be considered to enhance the light utilization efficiency from an engineering standpoint. (3) Microstructure regulation, degradation pathway of organic contaminants and toxicity reduction should be further investigated in wastewater remediation applications. The balance between mineralization degree of organic contaminants, toxicity reduction andeconomic cost should be further evaluated. The theoretical guidance and experimental basis for exploitation of efficient sulfide-based Z-scheme heterojunctions, degradation, and toxicity reduction of organic pollutants should be explored. (4) The proper regeneration methods should be further explored for enhancement of long-term stability of photo- catalytic reactors and their extension of service life in engineering application.

Declaration of competing interest

The authors declare that they have no known competing financialinterests or personal relationships that could have appeared to influence the work reported in this paper.

Data availability

Data will be made available on request.

Acknowledgments

This work was financially supported by the Natural Science Foun- dation of China (51978324, 51720105001, 51962023), Jiangxi Aca- demic and Technical Leader of Major Disciplines (20213BCJL22053) and Department of Education Fund of Jiangxi Province (GJJ210913).

References

Ahluwalia, S., Prakash, N., Prakash, R., Pal, B., 2016. Improved degradation of methyl orange dye using bio-co-catalyst Se nanoparticles impregnated ZnS photocatalyst under UV irradiation. Chem. Eng. J. 306, 1041–1048. https://doi.org/10.1016/j. cej.2016.08.028.

Ai, Z., Zhao, G., Zhong, Y., Shao, Y., Huang, B., Wu, Y., Hao, X., 2018. Phase junction CdS: high efficient and stable photocatalyst for hydrogen generation. Appl. Catal. B Environ. 221, 179–186. https://doi.org/10.1016/j.apcatb.2017.09.002.

Albero, J., Peng, Y., García, H., 2020. Photocatalytic CO_2 reduction to C2 products. ACS Catal. 10, 5734–5749. https://doi.org/10.1021/acscatal.0c00478.

Alberto, N., Altomare, M., Zoppellaro, G., Liu, N., Kment, Š., Zbořil, R., Schmuki, P., 2018. Photocatalysis with reduced TiO_2: from black TiO_2 to cocatalyst-free hydrogen production. ACS Catal. 9, 345–364. https://doi.org/10.1021/acscatal.8b04068.

Cai, T., Liu, Y., Wang, L., Dong, W., Zeng, G., 2019. Recent advances in round-the-clock photocatalytic system: mechanisms, characterization techniques and applications.
J. Photochem. Photobiol., C 39, 58–75. https://doi.org/10.1016/j. jphotochemrev.2019.03.002.

Chandrasekaran, S., Yao, L., Deng, L., Bowen, C., Zhang, Y., Chen, S., Lin, Z., Deng, Fang, Zhang, P., 2019. Recent advances in metal sulfides: from controlled fabrication to electrocatalytic, photocatalytic and photoelectrochemical water splitting and beyond. Chem. Soc. Rev. 48, 4178–4280. https://doi.org/10.1039/C8CS00664D.

Chauhan, D.K., Battula, V.R., Jain, S., Kailasam, K., 2021. Photocatalytic integrated production of hydrogen and imines from aromatic amines via Ni-mesoporous carbon nitride: an acceptorless dehydrogenative pathway. J. Clean. Prod. 307, 127162 https://doi.org/10.1016/j.jclepro.2021.127162.

Chen, S., Vequizo, J.J.M., Pan, Z., Hisatomi, T., Nakabayashi, M., Lin, L., Wang, Z., Kato, K., Yamakata, A., Shibata, N., Takata, T., Yamada, T., Domen, K., 2021. Surface modifications of $(ZnSe)_{0.5}(CuGa_{2.5}Se_{4.25})_{0.5}$ to promote photocatalytic Z-scheme overall water splitting. J. Am. Chem. Soc. 143, 10633–10641. https://doi.org/ 10.1021/jacs.1c03555.

Cheng, L., Xiang, Q., Liao, Y., Zhang, H., 2018. CdS-based photocatalysts. Energy Environ. Sci. 11, 1362–1391. https://doi.org/10.1039/C7EE03640J.

Cheng, L., Zhang, Y., Fan, W., Ji, Y., 2022. Synergistic adsorption-photocatalysis for dyes removal by a novel biochar-based Z-scheme heterojunction BC/2ZIS/WO_3: mechanistic investigation and degradation pathways. Chem. Eng. J. 445, 136677 https://doi.org/10.1016/j.cej.2022.136677.

Dashtian, K., Ghaedi, M., Shirinzadeh, H., Hajati, S., Shahbazi, S., 2018. Achieving enhanced blue-light-driven photocatalysis using nanosword-like $VO_2/CuWO_4$ type IIn-n heterojunction. Chem. Eng. J. 339, 189–203. https://doi.org/10.1016/j. cej.2018.01.107.

Deng, F., Lu, X., Luo, Y., Wang, J., Che, W., Yang, R., Luo, X., Luo, S., Dionysiou, D.D., 2019. Novel visible-light-driven direct Z-scheme $CdS/CuInS_2$ nanoplates for excellent photocatalytic degradation performance and highly-efficient Cr(VI) reduction. Chem. Eng. J. 361, 1451–1461. https://doi.org/10.1016/j. cej.2018.10.176.

Deng, F., Luo, Y., Li, H., Xia, B., Luo, X., Luo, S., 2020. Efficient toxicity elimination ofaqueous Cr(VI) by positively-charged $BiOCl_xI_{1-x}$, $BiOBr_xI_{1-x}$ and $BiOCl_xBr_{1-x}$ solid solution with internal hole-scavenging capacity via the synergy of adsorption and photocatalytic reduction. J. Hazard Mater. 383, 121127 https://doi.org/10.1016/j. jhazmat.2019.121127.

Fang, Y., Zheng, Y., Fang, T., Chen, Y., Zhu, Y., Liang, Q., Sheng, H., Shao, Z., 2020. Photocatalysis: an overview of recent developments and technological advancements. Sci. China Chem. 63, 149–181. https://doi.org/10.1007/s11426- 019-9655-0.

Feng, S., Chen, T., Liu, Z., Shi, J., Yue, X., Li, Y., 2020. Z-scheme CdS/CQDs/g-C_3N_4 composites with visible-near-infrared light response for efficient photocatalytic organic pollutant degradation. Sci. Total Environ. 704, 135404 https://doi.org/ 10.1016/j.scitotenv.2019.135404.

Feng, Y.X., Wang, H.J., Wang, J.W., Zhang, W., Zhang, M., Lu, T.B., 2021. Stand-alone CdS nanocrystals for photocatalytic CO_2 reduction with high efficiency and selectivity. ACS Appl. Mater. Interfaces 13, 26573–26580. https://pubs.acs.org/doi/ 10.1021/acsami.1c03606.

Friedrich, D., Schlosser, M., Pfitzner, A., 2017. Interconversion of one-dimensional thiogallates $Cs_2[Ga_2(S_2)_{2-x}S_{2x}]$ (x 0, 1, 2) by using high-temperature decomposition and polysulfide-flux reactions. Cryst. Growth Des. 17, 4887–4892. https://doi.org/10.1021/acs.cgd.7b00840.

Ganguly, P., Mathew, S., Clarizia, L., Kumar R, S., Akande, A., Hinder, S.J., Breen, A.,Pillai, S.C., 2019a. Ternary metal chalcogenide heterostructure $(AgInS_2\text{-}TiO_2)$ nanocomposites for visible light photocatalytic applications. ACS Omega 5, 406–421. https://doi.org/10.1021/acsomega.9b02907.

Ganguly, P., Mathew, S., Clarizia, L., Akande, A., Hinder, S., Breen, A., Pillai, S.C., 2019b. Theoretical and experimental investigation of visible light responsive $AgBiS_2\text{-}TiO_2$ heterojunctions for enhanced photocatalytic applications. Appl. Catal. B Environ. 253, 401–418. https://doi.org/10.1016/j.apcatb.2019.04.033.

Ganguly, P., Harb, M., Cao, Z., Cavallo, L., Breen, A., Dervin, S., Dionysiou, D.D., Pillai, S.C., 2019c. 2D nanomaterials for photocatalytic hydrogen production. ACS Energy Lett. 4, 1687–1709. https://doi.org/10.1021/acsenergylett.9b00940.

Ganguly, P., Muscetta, M., Padmanabhan, N.T., Clarizia, L., Akande, A., Hinder, S., Mathew, S., John, H., Breen, A., Pillai, S.C., 2021. New insights into the efficient charge transfer of ternary chalcogenides composites of TiO_2. Appl. Catal. B Environ. 282, 119612 https://doi.org/10.1016/j.apcatb.2020.119612.

Gao, B., Pan, Y., Chang, Q., Xi, Z., Yang, H., 2022. Hierarchically Z-scheme photocatalyst of {010} $BiVO_4$/Ag/CdS with enhanced performance in synergistic adsorption- photodegradation of fluoroquinolones in water. Chem. Eng. J. 435, 134834.

Gautam, A.K., Faraz, M., Khare, N., 2020. Enhanced thermoelectric properties of MoS_2 with the incorporation of reduced graphene oxide (RGO). J. Alloys Compd. 838, 155673 https://doi.org/10.1016/j.jallcom.2020.155673.

Guo, Y., Yan, B., Deng, F., Shao, P., Zou, J., Luo, X., Zhang, Z., Li, X., 2023. Lattice expansion boosting photocatalytic degradation performance of $CuCo_2S_4$ with aninherent dipole moment. Chin. Chem. Lett. https://doi.org/10.1016/j. cclet.2022.04.066.

Hao, Q., Wang, Z., Wang, T., Ren, Z., Zhou, C., Yang, X., 2018. Role of Pt loading in the photocatalytic chemistry of methanol on rutile TiO_2 (110). ACS Catal. 9, 286–294. https://doi.org/10.1021/acscatal.8b03359.

Hao, C., Tang, Y., Shi, W., Chen, F., Guo, F., 2021. Facile solvothermal synthesis of a Z- Scheme 0D/3D $CeO_2/ZnIn_2S_4$ heterojunction with enhanced photocatalytic performance under visible light irradiation. Chem. Eng. J. 409, 128168 https://doi. org/10.1016/j.cej.2020.128168.

He, Y., Zhang, L., Teng, B., Fan, M., 2015. New application of Z-Scheme Ag_3PO_4/g-C_3N_4 composite in converting CO_2 to fuel. Environ. Sci. Technol. 49, 649–656. https://doi. org/10.1021/es5046309.

https://dst.gov.in/large-scale-reactor-developed-cost-effective-production-hydrogen-u sing-sunlight-and-water.

Hu, J., Liu, A., Jin, H., Ma, D., Yin, D., Ling, P., Wang, S., Lin, Z., Wang, J., 2015. A versatile strategy for shish-kebab-like multi-heterostructured chalcogenides and enhanced photocatalytic hydrogen evolution. J. Am. Chem. Soc. 137, 11004–11010. https://doi.org/10.1021/jacs.5b04784.

Hu, X., Deng, F., Huang, W., Zeng, G., Luo, X., Dionysiou, D.D., 2018. The band structure control of visible-light-driven rGO/ZnS-MoS_2 for excellent photocatalytic degradation performance and long-term stability. Chem. Eng. J. 350, 248–256. https://doi.org/10.1016/j.cej.2018.05.182.

Hua, X., Chen, H., Rong, C., Addison, F., Dong, D., Qu, J., Liang, D., Guo, Z., Zheng, N.,Liu, H., 2023. Visible-light-driven photocatalytic degradation of tetracycline hydrochloride by Z-scheme Ag_3PO_4/1T@2H-MoS_2 heterojunction: degradation mechanism, toxicity assessment, and potential applications. J. Hazard Mater. 448, 130951 https://doi.org/10.1016/j.jhazmat.2023.130951.

Huang, D., Yan, X.L., Yan, M., Zeng, G.M., Zhou, C.Y., Wan, J., Cheng, M., Xu, W.J., 2018. Graphitic carbon nitride-based heterojunction photoactive nanocomposites: applications and mechanism insight. ACS Appl. Mater. Interfaces 10, 21035–21055. https://doi.org/10.1021/acsami.8b03620.

Jiang, G., 2016. Preface to the special topic on environmental pollution and health risk. Natl. Sci. Rev. 3, 409. https://doi.org/10.1093/nsr/nww090.

Jiang, R., Lu, G., Nkoom, M., Yan, Z., Wu, D., Liu, J., Dang, T., 2020. Mineralization and toxicity reduction of the benzophenone-1 using 2D/2D Cu_2WS_4/BiOCl Z-scheme system: simultaneously improved visible-light absorption and charge transfer efficiency. Chem. Eng. J. 400, 125913 https://doi.org/10.1016/j.cej.2020.125913.

Jin, J., Yu, J., Guo, D., Cui, C., Ho, W., 2015. A hierarchical Z-scheme CdS-WO_3 photocatalyst with enhanced CO_2 reduction activity. Small 11, 5262–5271. https:// doi.org/10.1002/smll.201500926.

Jin, Z., Zeng, S., Cao, C., Ma, H., Sun, D., 2020. Impacts of pollution abatement projects on happiness: an exploratory study in China. J. Clean. Prod. 274, 122869 https:// doi.org/10.1016/j.jclepro.2020.122869.
Kim, J.H., B, S., Min, B.K., 2020. Impact of absorber layer morphology on photovoltaic properties in solution-processed chalcopyrite solar cells. ACS Appl. Mater. Interfaces 13, 34–47. https://doi.org/10.1021/acsami.0c17496.
Lai, C., Lu, M., Chen, L., 2012. Metal sulfide nanostructures: synthesis, properties and applications in energy conversion and storage. J. Mater. Chem. 22, 19–30. https:// doi.org/10.1039/C1JM13879K.
Lee, G.J., Wu, J.J., 2017. Recent developments in ZnS photocatalysts from synthesis to photocatalytic applications-A review. Powder Technol. 318, 8–22. https://doi.org/ 10.1016/j.powtec.2017.05.022.
Lee, J., Kim, H., Lee, T., Jang, W., Lee, K.H., Soon, A., 2019. Revisiting polytypism in hexagonal ternary sulfide $ZnIn_2S_4$ for photocatalytic hydrogen production within the
Z-Scheme. Chem. Mater. 31, 9148–9155. https://doi.org/10.1021/acs. chemmater.9b03539.
Li, W., Feng, C., Dai, S., Yue, J., Hua, F., Hou, H., 2015. Fabrication of sulfur-doped g-C_3N_4/Au/CdS Z-scheme photocatalyst to improve the photocatalytic performance under visible light. Appl. Catal. B Environ. 168, 465–471. https://doi.org/10.1016/j. apcatb.2015.01.012.
Li, K., Peng, B., Peng, T., 2016a. Recent advances in heterogeneous photocatalytic CO_2 conversion to solar fuels. ACS Catal. 6, 7485–7527. https://doi.org/10.1021/ acscatal.6b02089.
Li, G., Su, R., Rao, J., Wu, J., Rudolf, P., Blake, G., Groot, R., Besenbacher, F., Palstra, T., 2016b. Band gap narrowing of SnS_2 superstructures with improved hydrogen production. J. Mater. Chem. 4, 209–216. https://doi.org/10.1039/C5TA07283B.
Li, H., Gao, Y., Zhou, Y., Fan, F., Han, Q., Xu, Qi, Wang, X., Xiao, M., Li, C., Zou, Z., 2016c. Construction and nanoscale detection of interfacial charge transfer of elegant Z-scheme WO_3/Au/In_2S_3 nanowire arrays. Nano Lett. 16, 5547–5552. https://doi. org/10.1021/acs.nanolett.6b02094.
Li, C., Yu, S., Che, H., Zhang, X., Han, J., Mao, Y., Wang, Y., Liu, C., Dong, H., 2018.
Fabrication of Z-scheme heterojunction by anchoring mesoporous γ-Fe_2O_3 nanospheres on g-C_3N_4 for degrading tetracycline hydrochloride in water. ACS Sustain. Chem. Eng. 6, 16437–16447. https://doi.org/10.1021/ acssuschemeng.8b03500.
Li, H., Deng, F., Zheng, Y., Hua, L., Qu, C., Luo, X., 2019a. Visible-light-driven Z-scheme rGO/Bi_2S_3-BiOBr heterojunctions with tunable exposed BiOBr (102) facets for efficient synchronous photocatalytic degradation of 2-nitrophenol and Cr(VI)
reduction. Environ. Sci.: Nano 6, 3670–3683. https://doi.org/10.1039/ C9EN00957D.
Li, G., Wang, B., Zhang, J., Wang, R., Liu, H., 2019b. Rational construction of a direct Z- scheme g-C_3N_4/CdS photocatalyst with enhanced visible light photocatalytic activity and degradation of erythromycin and tetracycline. Appl. Surf. Sci. 478, 1056–1064. https://doi.org/10.1016/j.apsusc.2019.02.035.
Li, C., Che, H., Yan, Y., Liu, C., Dong, H., 2020a. Z-scheme $AgVO_3$/$ZnIn_2S_4$ photocatalysts: "One Stone and Two Birds" strategy to solve photocorrosion and improve the photocatalytic activity and stability. Chem. Eng. J. 398, 125523 https:// doi.org/10.1016/j.cej.2020.125523.
Li, D., Kassymova, M., Cai, X., Zang, S., Jiang, H., 2020b. Photocatalytic CO_2 reduction over metal-organic framework-based materials. Coord. Chem. Rev. 412, 213262 https://doi.org/10.1016/j.ccr.2020.213262.
Li, Z.T., T Xu, X., Sheng, X.R., Lin, P., Tang, J., Pan, L.K., Kaneti, Y.V., Yang, T., Yamauchi, Y., 2021a. Solar-powered sustainable water production: state-of-the-art technologies for sunlight-energy-water nexus. ACS Nano 15, 12535–12566. https:// doi.org/10.1021/acsnano.1c01590.
Li, X., Kang, B., Dong, F., Zhang, Z., Luo, X., Han, L., Huang, J., Feng, Z., Chen, Z., Xu, J., Peng, B., Wang, Z., 2021b. Enhanced photocatalytic degradation and H_2/H_2O_2 production performance of S-pCN/$WO_{2.72}$ S-scheme heterojunction with appropriate surface oxygen vacancies. Nano Energy 81, 105671. https://doi.org/10.1016/j. nanoen.2020.105671.
Li, B., Wang, W., Zhao, J., Wang, Z., Su, B., Hou, Y., Ding, Z., Ong, W.-J., Wang, S., 2021c. All-solid-state direct Z-scheme $NiTiO_3/Cd_{0.5}Zn_{0.5}S$ heterostructures for photocatalytic hydrogen evolution with visible light. J. Mater. Chem. 9, 10270 https://doi.org/10.1039/D1TA01220G.
Li, X., Kang, B., Dong, F., Zhang, Z., Luo, X., Han, L., Huang, J., Feng, Z., Chen, Z., Xu, J., Peng, B., Wang, Z.L., 2021d. Enhanced photocatalytic degradation and H_2/H_2O_2 production performance of S-pCN/$WO_{2.72}$ S-scheme heterojunction with appropriate surface oxygen vacancies. Nano Energy 81, 105671. https://doi.org/10.1016/j. nanoen.2020.105671.
Li, B., Wang, W., Zhao, J., Wang, Z., Su, B., Hou, Y., Ding, Z., Ong, W., Wang, S., 2021e.
All-solid-state direct Z-scheme $NiTiO_3/Cd_{0.5}Zn_{0.5}S$ heterostructures for photocatalytic hydrogen evolution with visible light. J. Mater. Chem. 9, 10270–10276. https://doi.org/10.1039/D1TA01220G.
Li, C., Zhu, D., Cheng, S., Zuo, Y., Wang, Y., Ma, C., Dong, H., 2022a. Recent research progress of bimetallic phosphides-based nanomaterials as cocatalyst for photocatalytic hydrogen evolution, Chin. Chem. Lett. 33, 1141–1153. https://doi. org/10.1016/j.cclet.2021.07.057.
Li, C., Su, N., Wu, H., Liu, C., Che, G., Dong, H., 2022b. Synergies of adjacent sites in atomically dispersed ruthenium toward achieving stable hydrogen evolution. Inorg. Chem. 61, 13453–13461. https://doi.org/10.1021/acs.inorgchem.2c01908.
Li, X., Liu, Q., Deng, F., Huang, J., Han, L., He, C., Chen, Z., Luo, Y., Zhu, Y., 2022c.
Double-defect-induced polarization enhanced OV-BiOBr/Cu2-xS high-low junction for boosted photoelectrochemical hydrogen evolution. Appl. Catal. B Environ. 314, 121502 https://doi.org/10.1016/j.apcatb.2022.121502.
Li, Y.H., Qi, M.Y., Tang, Z.R., Xu, Y.J., 2022d. Coupling organic synthesis and hydrogen evolution over composite WO_3/$ZnIn_2S_4$ Z-Scheme photocatalyst. J. Phys. Chem. C126, 1872–1880. https://doi.org/10.1021/acs.jpcc.1c10911.
Li, Z., Chen, H., Li, Y., Wang, H., Liu, Y., Li, X., Lin, H., Li, S., Wang, L., 2022e. Porous direct Z-scheme heterostructures of S-deficient CoS/CdS hexagonal nanoplates for robust photocatalytic H_2 generation. CrystEngComm 24, 404–416. https://doi.org/ 10.1039/D1CE01453F.
Liang, S., Han, B., Liu, X., Chen, W., Peng, M., Guan, G., Deng, H., Lin, Z., 2018a. 3D spatially branched hierarchical Z-scheme CdS-Au nanoclusters-ZnO hybrids with boosted photocatalytic hydrogen evolution. J. Alloys Compd. 754, 105–113. https:// doi.org/10.1016/j.jallcom.2018.04.202.
Liang, M., Borjigin, T., Zhang, Y., Liu, H., Liu, B., Guo, H., 2018b. Z-Scheme Au@Void@ g-C_3N_4/SnS yolk shell heterostructures for superior photocatalytic CO_2 reduction under visible light. ACS Appl. Mater. Interfaces 10, 34123–34131. https://doi.org/ 10.1021/acsami.8b09455.
Lin, Z., Zheng, Y., Deng, F., Luo, X., Zou, J., Shao, P., Zhang, S., Tang, H., 2021. Target- directed design of dual-functional Z-scheme $AgIn_5S_8$/SnS_2 heterojunction for Pb(II) capture and photocatalytic reduction of Cr(VI): performance and mechanism insight. Sep. Purif. Technol. 277, 119430 https://doi.org/10.1016/j.seppur.2021.119430.
Loeb, S.K., Alvarez, P.J., Brame, J.A., Cates, E.L., Choi, W., Crittenden, J., Dionysiou, D.
D., Li, Q.L., Li-Puma, G., Xie, Q., Sedlak, D.L., Waite, T.D., Westerhoff, P., Kim, J., 2019. The technology horizon for photocatalytic water treatment: sunrise or sunset? Environ. Sci. Technol. 53, 2937–2947. https://doi.org/10.1021/acs.est.8b05041.
Low, J., Yu, J., Jaroniec, M., Wageh, S., Ai-Ghamdi, A.A., 2017. Heterojunction photocatalysts. Adv. Mater. 29, 1601694 https://doi.org/10.1002/ adma.201601694.
Lu, X., Che, W., Hu, X., Wang, Y., Zhang, A., Deng, F., Luo, S., Dionysiou, D.D., 2019. The facile fabrication of novel visible-light-driven Z-scheme $CuInS_2$/Bi_2WO_6 heterojunction with intimate interface contact by in situ hydrothermal growth strategy for extraordinary photocatalytic performance. Chem. Eng. J. 356, 819–829. https://doi.org/10.1016/j.cej.2018.09.087.
Luo, J., Zhou, X., Ma, L., Xu, L., Xu, X., Du, Z., Zhang, J., 2016. Enhancing visible light photocatalytic activity of direct Z-scheme SnS_2/Ag_3PO_4 heterojunction
photocatalysts. Mater. Res. Bull. 81, 16–26. https://doi.org/10.1016/j. materresbull.2016.04.028.
Luo, J., Zhang, X., Lu, J., Zhang, J., 2017a. Fine tuning the redox potentials of carbazolic porous organic frameworks for visible-light photoredox catalytic degradation of lignin β-O-4 models. ACS Catal. 7, 5062–5070. https://doi.org/10.1021/ acscatal.7b01010.
Luo, J., Zhou, X., Ning, X., Zhan, L., Ma, L., Xu, X., Huang, Z., Liang, J., 2017b. Synthesis and characterization of Z-scheme In_2S_3/Ag_2CrO_4 composites with an enhanced visible-light photocatalytic performance. New J. Chem. 41, 845–856. https://doi. org/10.1039/C6NJ02934E.
Lv, Y., Liu, H., Jin, D., Yang, H., He, D., Zhang, Z., Zhang, Y., Qu, J., Zhang, Y., 2022.
Effective degradation of norfloxacin on Ag_3PO_4/CNTs photoanode: Z-scheme mechanism, reaction pathway, and toxicity assessment. Chem. Eng. J. 429, 132092 https://doi.org/10.1016/j.cej.2021.132092.
Ma, Y., Zhang, Z., Jiang, X., Sun, R., Xie, M., Han, W., 2021. Direct Z-scheme Sn-In_2O_3/ In_2S_3 heterojunction nanostructures for enhanced photocatalytic CO_2 reduction activity. J. Mater. Chem. C 9, 3987. https://doi.org/10.1039/D1TC00014D.
Madhusudan, P., Shi, R., Xiang, S., Jin, M., Chandrashekar, B.N., Wang, J., Wang, W., Peng, O., Amini, A., Cheng, C., 2021. Construction of highly efficient Z-scheme $Zn_xCd_{1-x}S$/Au@ g-C_3N_4 ternary heterojunction composite for visible-light-driven photocatalytic reduction of CO_2 to solar fuel. Appl. Catal. B Environ. 282, 119600 https://doi.org/10.1016/j.apcatb.2020.119600.
Mao, M., Xu, J., Yu, X., Liu, Y., 2020. A Z-type heterojunction of bimetal sulfide $CuNi_2S_4$ and $CoWO_4$ for catalytic hydrogen evolution. Dalton Trans. 49, 6457–

6470. https:// doi.org/10.1039/D0DT00854K.
Meng, X., Liu, L., Ouyang, S., Xu, H., Wang, D., Zhao, N., ye, J., 2016. Nanometals for solar-to-chemical energy conversion: from semiconductor-based photocatalysis to plasmon-mediated photocatalysis and photo-thermocatalysis. Adv. Mater. 28, 6781–6803. https://doi.org/10.1002/adma.201600305.
Min, Y., He, G., Xu, Q., Chen, Y., 2014. Self-assembled encapsulation of graphene oxide/ Ag@AgCl as a Z-scheme photocatalytic system for pollutant removal. J. Mater. Chem. 2, 1294–1301. https://doi.org/10.1039/C3TA13687F.
Murugalakshmi, M., Jones, B.F., Mamba, G., Muruthamani, D., Muthuraj, V., 2021. Unravelling the visible light-assisted catalytic prowess of an n-n type In_2S_3/CeO_2 Z-scheme heterojunction towards organic and inorganic water pollution mitigation. New J. Chem. 45, 4046–4060. https://doi.org/10.1039/D0NJ04844E.
Ng, B.J., Putri, L.K., Kong, X.Y., Pasbakhsh, P., Chai, S.P., 2021. Z-scheme photocatalyst sheets with P-doped twinned $Zn_{0.5}Cd_{0.5}S_{1-x}$ and Bi_4NbO_8Cl connected by carbon electron mediator for overall water splitting under ambient condition. Chem. Eng. J. 404, 127030 https://doi.org/10.1016/j.cej.2020.127030.
Ong, W.J., Tan, L.L., Ng, Y.H., Yong, S.T., Chai, S.P., 2016. Graphitic carbon nitride ($g-C_3N_4$)-based photocatalysts for artificial photosynthesis and environmental remediation: are we a step closer to achieving sustainability? Chem. Rev. 116, 7159–7329. https://doi.org/10.1021/acs.chemrev.6b00075.
Osterloh, F.E., 2018. Journal of Materials Chemistry A Editor's choice web collection: "Recent advances in solar fuels and photocatalysis research". J. Mater. Chem. A. 6, 9763–9764. https://doi.org/10.1039/C8TA90108B.
Ouyang, C., Quan, X., Zhang, C., Pan, Y., Li, X., Hong, Z., Zhi, M., 2021a. Direct Z-scheme $ZnIn_2S_4$@MoO_3 heterojunction for efficient photodegradation of tetracycline hydrochloride under visible light irradiation. Chem. Eng. J. 424, 130510 https://doi. org/10.1016/j.cej.2021.130510.
Ouyang, C., Quan, X., Zhang, C., Pan, Y., Li, X., Hong, Z., Zhi, M., 2021b. Direct Z-scheme $ZnIn_2S_4$@ MoO_3 heterojunction for efficient photodegradation of tetracycline hydrochloride under visible light irradiation. Chem. Eng. J. 424, 130510 https://doi. org/10.1016/j.cej.2021.130510.
Pan, Y., You, Y., Xin, S., Li, Y., Fu, G., Cui, Z., Men, Y., Cao, F., Yu, S., Goodenough, J.B., 2017. Photocatalytic CO_2 reduction by carbon-coated indium-oxide nanobelts. J. Am. Chem. Soc. 139, 4123–4129. https://doi.org/10.1021/jacs.7b00266.
Paul, T., Das, D., Das, B.K., Sarkar, S., Maiti, S., Chattopadhyay, K.K., 2019. $CsPbBrCl_2$/g- C_3N_4 type II heterojunction as efficient visible range photocatalyst. J. Hazard Mater. 380, 120855 https://doi.org/10.1016/j.jhazmat.2019.120855.
Pillai, S.C., Kumaravel, V., 2021. Photocatalysis. De Gruyter, Berlin, Boston. https://doi. org/10.1515/9783110668483.
Qi, J., Zhang, W., Cao, R., 2018. Solar-to-hydrogen energy conversion based on water splitting. Adv. Energy Mater. 8, 1701620 https://doi.org/10.1002/ aenm.201701620.
Qiu, B., Zhu, Q., Du, M., Fan, L., Xing, M., Zhang, J., 2017a. Efficient solar light harvesting CdS/Co_9S_8 hollow cubes for z-scheme photocatalytic water splitting. Angew. Chem. Int. Ed. 56, 2684–2688. https://doi.org/10.1002/anie.201612551.
Qiu, F., Li, W., Wan, F., Li, H., Liu, X., Sun, J., 2017b. In-situ synthesis of novel Z-scheme $SnS_2/BiOBr$ photocatalysts with superior photocatalytic efficiency under visible light. J. Colloid Interface Sci. 493, 1–9. https://doi.org/10.1016/j.jcis.2016.12.066.
Ran, J., Jaroniec, M., Qiao, S., 2018. Cocatalysts in semiconductor-based photocatalytic CO_2 reduction: achievements, challenges, and opportunities. Adv. Mater. 30, 1704649 https://doi.org/10.1002/adma.201704649.
Raza, A., Shen, H., Haidry, A.A., Sun, L., Liu, R., Cui, S., 2020. Studies of Z-scheme WO_3- TiO_2/Cu_2ZnSnS_4 ternary nanocomposite with enhanced CO_2 photoreduction under visible light irradiation. J. CO2 Util. 37, 260–271. https://doi.org/10.1016/j. jcou.2019.12.020.
Ren, Y., Zeng, D., Ong, W.J., 2019. Interfacial engineering of graphitic carbon nitride ($g-C_3N_4$)-based metal sulfide heterojunction photocatalysts for energy conversion: a review. Chin. J. Catal. 40, 289–319. https://doi.org/10.1016/S1872-2067(19) 63293-6.
Ruan, X., Hu, H., Che, H., Jiang, E., Zhang, X., Liu, C., Che, G., 2019. A visible-light- driven Z-scheme $CdS/Bi_{12}GeO_{20}$ heterostructure with enhanced photocatalytic degradation of various organics and the reduction of aqueous Cr(VI). J. Colloid Interface Sci. 543, 317–327. https://doi.org/10.1016/j.jcis.2019.02.052.
Saravanakumar, K., Yun, K., Maheskumar, V., Yea, Y., Jagan, G., Park, C.M., 2023. Construction of novel In_2S_3/Ti_3C_2 MXene quantum dots/$SmFeO_3$ Z-scheme heterojunctions for efficient photocatalytic removal of sulfamethoxazole and 4-chlorophenol: degradation pathways and mechanism insights. Chem. Eng. J. 451, 138933 https://doi.org/10.1016/j.cej.2022.138933.
Scheuermann, A.G., McIntyre, P.C., 2016. Atomic layer deposited corrosion protection: apath to stable and efficient photoelectrochemical cells. J. Phys. Chem. Lett. 7, 2867–2878. https://doi.org/10.1021/acs.jpclett.6b00631.
Sharma, S.K., Kumar, A., Sharma, G., Stadler, F., Naushad, M., Ghfar, A., Ahamad, T., 2020. $LaTiO_2N/Bi_2S_3$ Z-scheme nano heterostructures modified by rGO with high interfacial contact for rapid photocatalytic degradation of tetracycline. J. Mol. Liq. 311, 113300 https://doi.org/10.1016/j.molliq.2020.113300.
Shen, S., Li, X., Zhou, Y., Han, L., Xie, Y., Deng, F., Huang, J., Chen, Z., Feng, Z., Xu, J., Dong, F., 2023. Novel $BiOBr/Bi_2S_3$ high-low junction prepared by molten salt method for boosting photocatalytic degradation and H_2O_2 production. J. Mater. Sci.Technol. 155, 148–159. https://doi.org/10.1016/j.jmst.2023.03.006.
Shi, L., Ma, Z., Qu, W., Zhou, W., Deng, Z., Zhang, H., 2021. Hierarchical Z-scheme Bi_2S_3/CdS heterojunction: controllable morphology and excellent photocatalytic antibacterial. Appl. Surf. Sci. 568, 150923 https://doi.org/10.1016/j. apsusc.2021.150923.
Shirakawa, T., Higashi, M., Tomita, O., Abe, R., 2017. Surface-modified metal sulfides as stable H_2-evolving photocatalysts in Z-scheme water splitting with a $[Fe(CN)_6]^{3-}/^{4-}$ redox mediator under visible-light irradiation. Sustain. Energy Fuels 1, 1065–1073. https://doi.org/10.1039/C7SE00151G.
Singh, S., Faraz, M., Khare, N., 2020. Recent advances in semiconductor-graphene and semiconductor-ferroelectric/ferromagnetic nanoheterostructures for efficient hydrogen generation and environmental remediation. ACS Omega 5, 11874–11882. https://doi.org/10.1021/acsomega.9b03913.
Sun, Q., Wang, N., Yu, J., Yu, J., 2018a. A hollow porous CdS photocatalyst. Adv. Mater. 30, 1804368 https://doi.org/10.1002/adma.201804368.
Sun, M., Zhao, B., Chen, F., Liu, C., Lu, S., Yu, Y., Zhang, B., 2018b. Thermally-assistedphotocatalytic CO_2 reduction to fuels. Chem. Eng. J. 6, 21056–21063. https://doi. org/10.1039/C8TA07352J.
Sun, D., Shao, S., Zhang, Y., Yang, Q., Hou, H., Quan, X., 2020. Integrated analysis of the water-energy-environmental pollutant nexus in the petrochemical industry. Environ. Sci. Technol. 54, 14830–14842. https://doi.org/10.1021/acs.est.9b07467.
Tian, Y., Zhou, Y., Zong, Y., Li, J., Yang, N., Zhang, M., Guo, Z., 2020. Construction of functionally compartmental inorganic photocatalyst-enzyme system via imitating chloroplast for efficient photoreduction of CO_2 to formic acid. ACS Appl. Mater. Interfaces 12, 34795–34805. https://doi.org/10.1021/acsami.0c06684.
Wageh, S., Al-Ghamdi, A., Jafer, R., Li, X., Zhang, P., 2021. A new heterojunction in photocatalysis: S-scheme heterojunction. Chin. J. Catal. 42, 667–669. https://doi. org/10.1016/s1872-2067(20)63705-6.
Wang, Y., Wang, Q., Zhan, X., Wang, F., Safdar, M., He, J., 2013. Visible light driven type II heterostructures and their enhanced photocatalysis properties: a review. Nanoscale 5, 8326–8339. https://doi.org/10.1039/C3NR01577G.
Wang, L., Cai, M.J., Sun, C.W., He, L., Zhang, X.H., 2018a. Promoting charge separation in semiconductor nanocrystal superstructures for enhanced photocatalytic activity. Adv. Mater. Interfac. 5, 1701694 https://doi.org/10.1002/admi.201701694.
Wang, Y., Liu, X., Liu, J., Han, B., Hu, X., Yang, F., Xu, Z., Li, Y., Jia, S., Li, Z., Zhao, Y., 2018b. Carbon quantum dot implanted graphite carbon nitride nanotubes: excellent charge separation and enhanced photocatalytic hydrogen evolution. Angew. Chem., Int. Ed. 57, 5765–5771. https://doi.org/10.1002/ange.201802014.
Wang, Y., Tian, Y., Lang, Z., Guan, W., Yan, L., 2018c. A highly efficient Z-scheme B- doped $g-C_3N_4/SnS_2$ photocatalyst for CO_2 reduction reaction: a computational study. J. Mater. Chem. 6, 21056 https://doi.org/10.1039/C8TA07352J.
Wang, P., Li, H., Sheng, Y., Chen, F., 2019a. Inhibited photocorrosion and improved photocatalytic H_2-evolution activity of CdS photocatalyst by molybdate

ions. Appl. Surf. Sci. 463, 27–33. https://doi.org/10.1016/j.apsusc.2018.08.125.
Wang, S., Zhu, B., Liu, M., Zhang, L., Yu, J., Zhou, M., 2019b. Direct Z-scheme ZnO/CdS hierarchical photocatalyst for enhanced photocatalytic H_2-production activity. Appl. Catal. B Environ. 243, 19–26. https://doi.org/10.1016/j.apcatb.2018.10.019.
Wang, X., Wang, X., Huang, J., Li, S., Meng, A., Li, Z., 2021a. Interfacial chemical bond and internal electric field modulated Z-scheme Sv-$ZnIn_2S_4$/$MoSe_2$ photocatalyst for efficient hydrogen evolution. Nat. Commun. 12, 1–11. https://doi.org/10.1038/ s41467-021-24511-z.
Wang, Z., Wang, Z., Zhu, X., Ai, C., Zeng, Y., Shi, W., Zhang, X., Zhang, H., Si, H., Li, J., Wang, C., Lin, S., 2021b. Photodepositing CdS on the active cyano groups decorated g-C_3N_4 in Z-scheme manner promotes visible-light-driven hydrogen evolution. Small 17, 2102699. https://doi.org/10.1002/smll.202102699.
Wang, L., Bie, C., Yu, J., 2022a. Challenges of Z-scheme photocatalytic mechanisms. Trends Chem 4, 973–983. https://doi.org/10.1016/j.trechm.2022.08.008.
Wang, G., Tang, Z., Wang, J., Lv, S., Xiang, Y., Li, F., Liu, C., 2022b. Energy band engineering of $Bi_2O_{2.33}$-CdS direct Z-scheme heterojunction for enhanced photocatalytic reduction of CO_2. J. Mater. Sci. Technol. 111, 17–27. https://doi.org/ 10.1016/j.jmst.2021.09.018.
Wang, M., Zeng, S., Woldu, A.R., Hu, L., 2022c. $BiVO_4$/Bi_2S_3 Z-scheme heterojunction with MnOx as a cocatalyst for efficient photocatalytic CO_2 conversion to methanol by pure water. Nano Energy 104, 107925. https://doi.org/10.1016/j. nanoen.2022.107925.
Wei, X., Zhang, X., Ali, S., Han, W., He, D., Wang, J., Kong, S., Feng, Z., Zhang, G., Qi, J., 2021. Elucidating the mechanistic origins of P dopants triggered active sites and direct Z-scheme charge transfer by P-MoS_2@WO_3 heterostructures for efficient photocatalytic hydrogen evolution. J. Alloys Compd. 872, 159637 https://doi.org/ 10.1016/j.jallcom.2021.159637.
Xi, Y., Chen, W., Dong, W., Fan, Z., Wang, K., Shen, Y., Tu, G., Zhong, S., Bai, S., 2021. Engineering an interfacial facet of s-scheme heterojunction for improved photocatalytic hydrogen evolution by modulating the internal electric field. ACS Appl. Mater. Interfaces 13, 39491–39500. https://doi.org/10.1021/ acsami.1c11233.
Xia, X., Pan, J.H., Pan, X., Hu, L., Yao, J., Ding, Y., Wang, D.F., Ye, J.H., Dai, S., 2019. Photochemical conversion and storage of solar energy. ACS Energy Lett. 4, 405–410. https://doi.org/10.1021/acsenergylett.8b02411.
Xia, B., Deng, F., Zhang, S., Hua, L., Luo, X., Ao, M., 2020. Design and synthesis of robust Z-scheme ZnS-SnS_2 n-n heterojunctions for highly efficient degradation of pharmaceutical pollutants: performance, valence/conduction band offset photocatalytic mechanisms and toxicity evaluation. J. Hazard Mater. 392, 122345 https://doi.org/10.1016/j.jhazmat.2020.122345.
Xiao, J., Li, J., Xu, Z., 2019. Challenges to future development of spent lithium ion batteries recovery from environmental and technological perspectives. Environ. Sci.Technol. 54, 9–25. https://doi.org/10.1021/acs.est.9b03725.
Xu, F., Meng, K., Zhu, B., Liu, H., Xu, J., Yu, J., 2019. Graphdiyne: a new photocatalytic CO_2 reduction cocatalyst. Adv. Funct. Mater. 29, 1904256 https://doi.org/10.1002/ adfm.201904256.
Xu, Q., Zhang, L., Cheng, B., Fan, J., Yu, J., 2020. S-scheme heterojunction photocatalyst. Chem 6, 1543–1559. https://doi.org/10.1016/j.chempr.2020.06.010.
Xu, C., Zhou, Q., Huang, W., Yang, K., Zhang, Y., Liang, T., Liu, Z., 2022a. Constructing Z-scheme β-Bi_2O_3/ZrO_2 heterojunctions with 3D mesoporous SiO_2 nanospheres for efficient antibiotic remediation via synergistic adsorption and photocatalysis. Rare Met. 41, 2094–2107. https://doi.org/10.1007/s12598-021-01897-9.
Xu, X., Deng, F., Shao, P., Dionysiou, D.D., Luo, X., Li, X., Zhang, S., Liu, X., Liu, M.,2022b. Internal electric field driving separation and migration of charge carriers via Z-scheme path in $AgIn_5S_8$/ZnO heterojunction for efficient decontamination of pharmaceutical pollutants. Chem. Eng. J. 428, 132096 https://doi.org/10.1016/j. cej.2021.132096.
Xu, Q., He, R., Li, Y., 2023. Problems and mistakes for electron transfer mechanism in Z- scheme photocatalytic system. Acta Phys. Chim. Sin. 39, 2211009 https://doi.org/ 10.3866/PKU.WHXB202211009.
Xue, Y., Wu, Z., He, X., Li, Q., Yang, X., Li, L., 2019. Hierarchical fabrication Z-scheme photocatalyst of $BiVO_4$(040)-Ag@CdS for enhanced photocatalytic properties under simulated sunlight irradiation. J. Colloid Interface Sci. 548, 293–302. https://doi. org/10.1016/j.jcis.2016.12.066.
Ye, X., Chen, Y., Ling, C., Zhang, J., Meng, S., Fu, X., Wang, X., Chen, S., 2018. Chalcogenide photocatalysts for selective oxidation of aromatic alcohols to aldehydes using O_2 and visible light: a case study of $CdIn_2S_4$, CdS and In_2S_3. Chem. Eng. J. 348, 966–977. https://doi.org/10.1016/j.cej.2018.05.035.
Yoshino, S., Iwase, A., Yamaguchi, Y., Suzuki, T.M., Morikawa, T., Kudo, A., 2022. Photocatalytic CO_2 reduction using water as an electron donor under visible light irradiation by Z-scheme and photoelectrochemical systems over $(CuGa)_{0.5}ZnS_2$ in the presence of basic additives. J. Am. Chem. Soc. 144, 2323–2332. https://doi.org/ 10.1021/jacs.1c12636.
Yu, X.Y., Yu, L., Lou, X.W.D., 2016. Metal sulfide hollow nanostructures for electrochemical energy storage. Adv. Energy Mater. 6, 1501333 https://doi.org/ 10.1002/aenm.201501333.
Yuan, X., Jiang, L., Chen, X., Leng, L., Wang, H., Wu, Z., Xiong, T., Liang, J., Zeng, G., 2017a. Highly efficient visible-light-induced photoactivity of Z-scheme Ag_2CO_3/Ag/ WO_3 photocatalysts for organic pollutant degradation. Environ. Sci.: Nano 4, 2175–2185. https://doi.org/10.1039/C7EN00713B.
Yuan, Y.J., Chen, D., Yang, S., Yang, L.X., Wang, J.J., Cao, D., Tu, W., Yu, Z.T., Zou, Z.G., 2017b. Constructing noble-metal-free Z-scheme photocatalytic overall water splitting systems using MoS_2 nanosheet modified CdS as a H_2 evolution photocatalyst. J. Mater. Chem. 5, 21205–21213. https://doi.org/10.1039/ C7TA06664A.
Yuan, Y., Chen, D., Yu, Z., Zou, Z., 2018. Cadmium sulfide-based nanomaterials for photocatalytic hydrogen production. J. Mater. Chem. 6, 11606–11630. https://doi. org/10.1039/C8TA00671G.
Zeng, Z., Mabe, T., Zhang, W., Bagra, B., Ji, Z.W., Yin, Z.Y., Allado, K., W, J.J., 2018a. Plasmon-exciton coupling in photosystem I based biohybrid photoelectrochemical cells. ACS Appl. Bio Mater. 1, 802–807. https://doi.org/10.1021/acsabm.8b00249.
Zeng, C., Hu, Y.M., Zhang, T.R., Dong, F., Zhang, Y.H., Huang, H.W., 2018b. A core–satellite structured Z-scheme catalyst $Cd_{0.5}Zn_{0.5}S$/$BiVO_4$ for highly efficient and stable photocatalytic water splitting. J. Mater. Chem. 6, 16932–16942. https:// doi.org/10.1039/c8ta04258f.
Zeng, C., Zeng, Q., Dai, C.H., Hu, Y.M., 2020. An oriented built-in electric field induced by cobalt surface gradient diffused doping in $MgIn_2S_4$ for enhanced photocatalytic CH_4 evolution. Dalton Trans. 49, 9213. https://doi.org/10.1039/d0dt01686a.
Zhang, L.J., Li, S., Liu, B.K., Wang, D.J., Xie, T.F., 2014. Highly efficient CdS/WO_3 photocatalysts: Z-Scheme photocatalytic mechanism for their enhanced photocatalytic H_2 evolution under visible light. ACS Catal. 4, 3724–3729. https:// doi.org/10.1021/cs500794j.
Zhang, L., Niu, C.G., Wen, X.J., Guo, H., Zhao, X.F., Liang, C., Zeng, G.M., 2018. Enhanced photocatalytic activity of CdS/SnS_2 nanocomposite with highly-efficient charge transfer and visible light utilization for selective reduction of 4-nitroaniline. J. Colloid Interface Sci. 532, 557–570. https://doi.org/10.1016/j.jcis.2018.08.017.
Zhang, X., Zhang, R., Niu, S., Zheng, J., Guo, C., 2019a. Construction of core-shell structured WO_3@SnS_2 hetero-junction as a direct Z-scheme photo-catalyst. J. Colloid Interface Sci. 554, 229–238. https://doi.org/10.1016/j.jcis.2019.06.107.
Zhang, Y., Hao, X., Ma, X., Liu, H., Jin, Z., 2019b. Special Z-scheme CdS@ WO_3 hetero- junction modified with CoP for efficient hydrogen evolution. Int. J. Hydrogen Energy 44, 13232–13241. https://doi.org/10.1016/j.jallcom.2018.04.202.
Zhang, Q., Liu, B., Ji, Y., Chen, L., Zhang, L., Li, L., Wang, C., 2020. Construction of hierarchical yolk-shell nanospheres organized by ultrafine Janus subunits for efficient overall water splitting. Nanoscale 12, 2578–2586. https://doi.org/10.1039/ C9NR08802D.
Zhang, E., Zhu, Q., Huang, J., Liu, J., Tan, G., Sun, C., Li, T., Liu, S., Liu, S., Li, Y., Wang, H., Wan, X., Wen, Z., Fan, F., Zhang, J., Ariga, K., 2021a. Visually resolving the direct Z-scheme heterojunction in CdS@$ZnIn_2S_4$ hollow cubes for photocatalytic evolution of H_2 and H_2O_2 from pure water. Appl. Catal. B Environ. 293, 120213 https://doi.org/10.1016/j.apcatb.2021.120213.
Zhang, L., Feng, L., Li, P., Chen, X., Gao, Y., Gong, Y., Du, Z., Zhang, S., Zhang, A., Chen, G., Wang, H., 2021b. Plasma-assisted doping of nitrogen into cobalt sulfide for loading cadmium sulfide: a direct Z-scheme heterojunction for efficiently photocatalytic Cr(VI) reduction under visible light. Chem. Eng. J. 417, 129222 https://doi.org/10.1016/j.cej.2021.129222.
Zhang, Y., Hu, L., Zhou, H., Wang, H., Zhang, Y., 2022. NIR photothermal-enhanced electrocatalytic and photoelectrocatalytic hydrogen evolution by polyaniline/SnS2 nanocomposites. ACS Appl. Nano Mater. 5, 391–400. https://doi.org/10.1021/ acsanm.1c03211.
Zhang, Z., Ji, R., Sun, Q., He, J., Chen, D., Li, N., Li, H., Marcomini, A., Xu, Q., Lu, J., 2023. Enhanced photocatalytic degradation of 2-chlorophenol over Z-scheme heterojunction of CdS-decorated oxygen-doped g-C_3N_4 under visible-light. Appl. Catal. B Environ. 324, 122276

https://doi.org/10.1016/j.apcatb.2022.122276.
Zhao, M., Zhao, Z., Wang, Z., Jiang, J., Yu, L., Cai, Z., 2021a. Well-designed $ZnIn_2S_4$/ TiO_2 Z-type heterojunction for efficient photocatalytic reduction of Cr(VI). Ceram. Int. 47, 25337–25342. https://doi.org/10.1016/j.ceramint.2021.05.255.
Zhao, W., Li, Y., Zhao, P., Zhang, L., Dai, B., Xu, J., Huang, H., He, Y., Leung, D.Y., 2021b. Novel Z-scheme Ag-C_3N_4/SnS_2 plasmonic heterojunction photocatalyst for degradation of tetracycline and H_2 production. Chem. Eng. J. 405, 126555 https:// doi.org/10.1016/j.cej.2020.126555.
Zhao, G., Hu, J., Long, X., Zou, J., Yu, J., Jiao, F., 2021c. A critical review on black phosphorus-based photocatalytic CO_2 reduction application. Small 17, 2102155. https://doi.org/10.1002/smll.202102155.
Zhao, J., Ji, M., Chen, H., Weng, Y.X., Zhong, J., Li, Y., Wang, S., Chen, Z., Xia, J., Li, H., 2022. Interfacial chemical bond modulated $Bi_{19}S_{27}Br_3$/g-C_3N_4 Z-scheme heterojunction for enhanced photocatalytic CO_2 conversion. Appl. Catal. B Environ. 307, 121162 https://doi.org/10.1016/j.apcatb.2022.121162.
Zhen, C., Wu, T.T., Chen, R., Wang, L.Z., Liu, G., Cheng, H.M., 2019. Strategies for modifying TiO_2 based electron transport layers to boost perovskite solar cells. ACS Sustain. Chem. Eng. 7, 4586–4618. https://doi.org/10.1021/ acssuschemeng.8b06580.
Zheng, A., Guo, T., Guan, F., Chen, X., Shu, Y., Wang, J., 2019. Ionic liquid mediated carbon dots: preparations, properties and applications. Trends Anal. Chem. 119, 115638 https://doi.org/10.1016/j.trac.2019.115638.
Zheng, X., Li, Y., Yang, J., Cui, S., 2021. Z-Scheme heterojunction Ag/NH_2-MIL-125 (Ti)/ CdS with enhanced photocatalytic activity for ketoprofen degradation: mechanism and intermediates. Chem. Eng. J. 422, 130105.
Zhou, Q., Huang, W., Xu, C., Liu, X., Yang, K., Li, D., Hou, Y., Dionysiou, D.D., 2021. Novel hierarchical carbon quantum dots-decorated BiOCl nanosheet/carbonized eggshell membrane composites for improved removal of organic contaminants from water via synergistic adsorption and photocatalysis. Chem. Eng. J. 420, 129582 https://doi.org/10.1016/j.cej.2021.129582.
Zhou, T., Zhang, P., Zhu, D., Cheng, S., Dong, H., Wang, Y., Che, G., Niu, Y., Yan, M., Li, C., 2022. Synergistic effect triggered by skeleton delocalization and edge induction of carbon nitride expedites photocatalytic hydrogen evolution. Chem. Eng. J. 442, 136190 https://doi.org/10.1016/j.cej.2022.136190.
Zhu, S., Wang, D., 2017. Photocatalysis: basic principles, diverse forms of implementations and emerging scientific opportunities. Adv. Energy Mater. 7, 1700841 https://doi.org/10.1002/aenm.201700841.
Zhu, D., Zhou, Q., 2021. Nitrogen doped g-C_3N_4 with the extremely narrow band gap for excellent photocatalytic activities under visible light. Appl. Catal. B Environ. 281, 119474 https://doi.org/10.1016/j.apcatb.2020.119474.
Zhu, L., Li, H., Liu, Z., Xia, P., Xie, Y., Xiong, D., 2018. Synthesis of the 0D/3D CuO/ZnO heterojunction with enhanced photocatalytic activity. J. Phys. Chem. C 122, 9531–9539. https://doi.org/10.1021/acs.jpcc.8b01933.
Zhu, Z., Wan, S., Zhao, Y., Qin, Y., Ge, X., Zhong, Q., Bu, Y., 2020. Recent progress in Bi_2WO_6-Based photocatalysts for clean energy and environmental remediation: competitiveness, challenges, and future perspectives. Nano Select 2, 1–29. https:// doi.org/10.1002/nano.202000127.
Zhu, H., Zhang, C., Xie, K., Li, X., Liao, G., 2023. Photocatalytic degradation of organic pollutants over MoS_2/Ag-$ZnFe_2O_4$ Z-scheme heterojunction: revealing the synergistic effects of exposed crystal facets, defect engineering, and Z-scheme mechanism. Chem. Eng. J. 453, 139775 https://doi.org/10.1016/j.cej.2022.139775.